REAL-TIME ARC FAULT DETECTION IN PHOTOVOLTAIC DC SYSTEMS

A Thesis

by

HEZI ZHU

Submitted to the Office of Graduate and Professional Studies of
Texas A&M University
in partial fulfillment of the requirements for the degree of

MASTER OF SCIENCE

Chair of Committee,	Robert S. Balog
Committee Members,	B. Don Russell
	Laszlo Kish
	Bimal Nepal
Head of Department,	Miroslav M. Begovic

May 2016

Major Subject: Electrical Engineering

Copyright 2016 Hezi Zhu

ABSTRACT

Arc fault is a significant reliability and safety concern for photovoltaic (PV) direct current (DC) electrical systems. Failure to detect an arc fault can lead to system failure, property loss, or even bodily injury. Of the numerous methods that have been proposed, the most common fast fourier transform (FFT) has significant fundamental limitations that stem from the fact that arcs do not conform to the inherent assumptions upon which the FFT is mathematically based. This can lead to the non-detection of arcing events, or the false-detection which is potentially just as bad as it leads to a reduced confidence in the technology and a better technology solution is needed. The goal of this research is to design and demonstrate a real-time, embedded system implementation of a new technique-wavelet transform (WT) for arc fault detection. In order to analyze arc of various power level under the intrinsic high frequency noise feature of PV systems, arc signals are synthesized with different Arc-Signal-Noise-Ratio (ASNR) and a high fidelity testbed is constructed for the reproduction of arc signals. With threshold setting simulated on MATLAB, WT detection technique using ratio of the power increment is realized on the commercial arc detection product RD-195. Real-time arc fault detection is conducted for both synthesized arc signal and real PV arc signal, and the detection result of the WT algorithm is compared against the FFT algorithm. From the experiment and analysis, the rationality of WT based detection technique for DC arc detection application is validated and the superiority compared to FFT technique is demonstrated.

ACKNOWLEDGEMENTS

It's a genuine pleasure to express my gratitude to my advisor and committee chair, Dr. Balog, for his expertise, support, and generous guidance throughout my graduate study.

I would also like to thank my committee members, Dr. Russell, Dr. Kish, and Dr. Nepal, for their valuable suggestions for my research.

I would like to extend my sincere gratitude to my friends Di Gao, Zhangxin Zhou, Stephen McConnell, Limeng Xie, Jiayun Li, and Lihua Liu for the hard time we've been through together; my colleagues in the Renewable Energy And Power Electronics Research Laboratory at Texas A&M University especially Zhan Wang, Xiao Li, and Haiyu Zhang for their assistance and encouragement; and the faculty and staff in Electrical and Computer Engineering Department for making my study at Texas A&M University a great experience.

Last of all, thanks to my mother and father, and boyfriend Yao for their selfless and consistent love, support, and encouragement.

TABLE OF CONTENTS

Page

LIST OF FIGURES

Page

LIST OF TABLES

Page

1. INTRODUCTION

1.1 Overview of arc faults on direct current (DC) photovoltaic systems

Photovoltaic (PV) energy is one of the most widely spread renewable energy source, and the usage has the rising tendency in recent years. Worldwide, PV systems are growing rapidly with more than 18% predicted rate and power increment from 35.9GW to 73.4GW up to the year of 2020 [1, 2]. However, the utilization of PV system not only brings clear energy, but also safety issues [3]. Arc fault is one of the major concerns for the safe operation of PV systems.

Arc is defined as the momentary partial discharge due to the intense concentration of a high-voltage electric field across a dielectric [4]. The occurrence of arc faults induces serious damages to PV systems[5]. It may precipitate the unstable operation or failure of the PV systems and the broken wire can pose electric shock hazard, further the heat generated from the discharge can ignite flammable materials in or around PV systems and develop electric fire, causing property loss and injury or even death to the building occupants [6]. In fact, several fire cases on PV systems have been reported claiming to be caused due to arc faults [7]. The PV panel fire shown in Figure 1 is an example.

Many facts contribute to the formation of arc faults [8, 9]. Poor connection of the metal joints and abrasion during installation, insulation deterioration because of the aging effect or corrosion, uncontrolled environmental influences such as rodent bites, humid weather condition like rain, etc, may all be part of the reason.

Figure 1 PV panel fire case taken from [10]

The occurrence of arc faults seems to be inevitable as it can take place anywhere in the PV systems. Connections in the array like inverters and inter-module connectors or connection between modules like junction boxes has high possibility where arc faults happen. PV systems which contain many conjunction joints and exposed cables are very susceptible to arc faults.

Depending on the location of occurrence, arc faults can be categorized into two types: serial and parallel arc [11-13]. Serial arcs are emerged due to the discontinuity of conduction path, and loose connection for instance [8], as introduced earlier. Breakdown and ionization of the gas in between the loosen conductors forms the path for the electrical arc. Parallel arcs are caused in between conductors of different potential, for example, line to line and line to ground [14]. As a diagram Figure 2 shows where arc faults happens in PV systems.

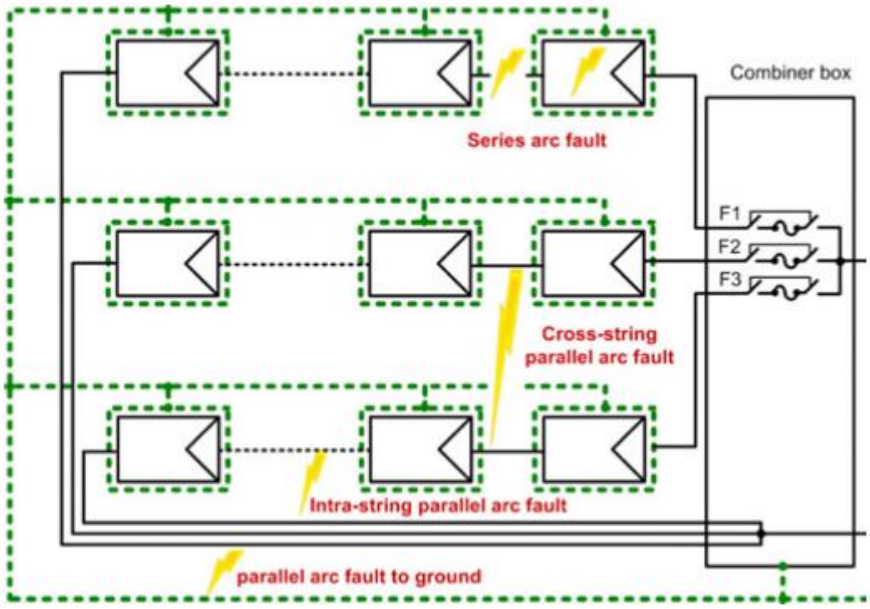

Figure 2 Arc faults location in PV systems taken from [11]

The appearance of arcs has below characteristics: on time domain it usually show voltage increment and current drop [15]; on frequency domain it looks random and like pink noise which suggest its magnitude is decreasing with increasing frequency value [16].

Different detection techniques were applied in literature. On alternative current (AC) systems, the zero current crossing [17, 18] can be utilized as a feature to recognize arc faults as arc needs to reignite when the AC current changes direction whereas direct current (DC) systems don't display such characteristic. Further, amplitude detection based on the current magnitude isn't effective as the current might not be enough to trigger the over current protection device or thermal circuit breaker. Detection scheme based on the variation of the current signal could be influenced by the existence of the inverter noise and doesn't apply either. Generally serial arc are considered more difficult to detect

compared to parallel faults, because series fault increases the system impedance causing the current drop and the arc might remain undetected by the over current protection device while parallel fault may exhibits current rise and could be more visible by the over current protector [19].

Alternatively, frequency spectrum is considered for the detection of arc and much research is devoted into this area. High frequency between 2kHz-10kHz [20] and low frequency between 30-360Hz [21] are both studied. In these method, arc is determined if frequency content within the band of interest relatively increased more than certain ratio. The random behavior of energy of the current signal [22] is also utilized for the determination of arc faults.

Due to the severe damage caused by arc faults, PV systems will be required to be equipped with arc faults detectors that detect both serial and parallel arc faults according to the 2011 National Electrical Code (NEC) [23]. Based on different detection techniques, many products or patent information about arc fault circuit interrupter (AFCI) [24, 25] and arc fault detector (AFD) [26-31] can be found online. Underwriters Laboratories (UL) also proposed UL1699B which describes requirements for the inventors of arc fault detectors to meet and tests to pass [32].

1.2 Problems encountered in frequency analysis based detection technique

Fourier transform (FT), defined in equation (1) is most widely used to analyze the frequency content of a signal [33].

$$X(\omega) = \int_{-\infty}^{\infty} x(t) e^{-j\omega t} dt \tag{1}$$

It convolves the signal with the transform operator $e^{-j\omega t}$ to derive the frequency content of the signal and the signal is viewed as the superimposition of a set of sine and cosine waves of different frequencies. A graphical representation of the superimposition process is shown in Figure 3. As shown in the graph, the Fourier Transform method has the limitation that the signal to be analyzed needs to be periodic.

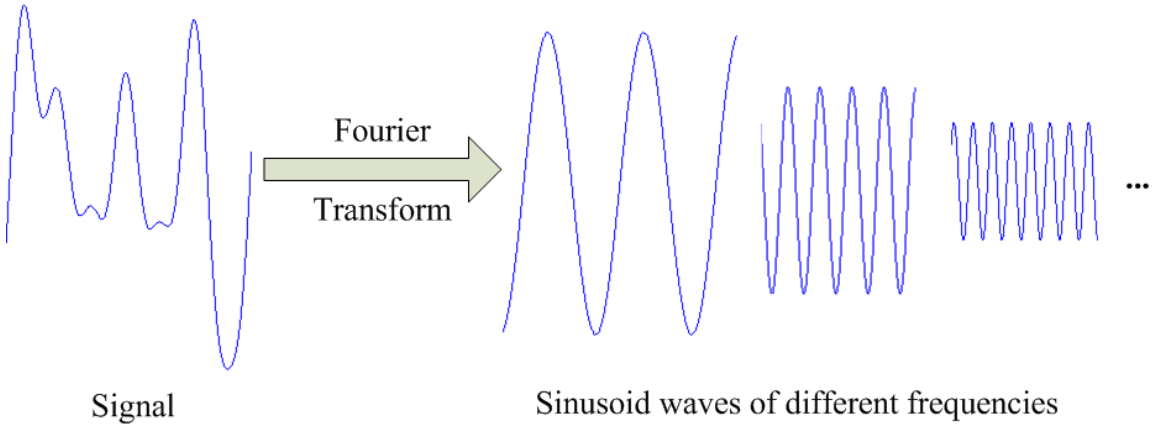

Figure 3 Graphical explanation of Fourier Transform

Expression for the Fourier Transform utilized in discrete systems- discrete fourier transform (DFT) can be found in equation (2):

$$X_k = \sum_{n=0}^{N-1} x_n e^{-j2\pi k \frac{n}{N}} \tag{2}$$

In DFT, frequency spectrum result has N output points which is the same length of input signal. The output represents amplitude and phase information of sine and cosine waves at different frequencies and the time domain signal in the sampling window can be represented using the derived frequency contents. Fast fourier transform (FFT) is the fast

computation algorithm for calculating DFT [34]. It reduces the computational complexity from the order of N^2 to $N \log N$, and hence is widely applied in real-time discrete system signal processing to reduce the stress on the hardware.

However there are several problems in the detection of arc faults using FT based technique [35]: first, FT requires stationary and periodic signal which is not the practical nature of arc signals; second, the frequency analysis resolution which also suggests the accuracy is dependent of the analysis window. Resolution of frequency domain analysis increases with window size but the temporal localization in the time domain suffers. In the real time detection if long data acquisition duration is required in order to obtain enough frequency resolution, the possibility of failing to localize the abnormal events arises. Therefore the trade-offs between time and frequency domain has to be made. Furthermore, the frequency resolution is not adjustable for different frequency band once the window size is fixed. It's usually desired to distinguish low frequency content with finer scale for arc signal as low frequency accounts for a large portion in arc signals. A necessity to meet the requirement of low frequency band analysis is either extending the window size or increasing the sampling rate. Drawbacks for the former solution is the analysis duration will be correspondingly prolonged and the possibility to miss the abnormal event in this duration increases as mentioned before. For the latter one, the hardware performance including Analog-Digital-Converter (ADC) and processor is expected to be improved can may introduce extra expenses. Therefore it might not be worthwhile considering the costs and complexity of the hardware system design. As an alternative to improve the temporal localization capability, short time fourier transform

(STFT) -another fourier transform based method is utilized to compute FFT based on several shorter window section [36]. It might solve the problem of fast localization whereas just like what've been explained, the accuracy of analyzation would be sacrificed [37]. Therefore, STFT is not ideal for analyzing abrupt disturbances nor short transient signals. As a conclusion, the fundamental drawback of trade-offs between time and frequency resolution for FFT based algorithm still remains unsolved.

Another complication of real arc fault detection on PV system is the intrinsic high frequency signal [11]. DC PV systems utilize large amount of dc/dc converters throughout the systems and the switching event of converters generate high frequency noises [38]. The existence of the high frequency noise obfuscates arc signal and increases the difficulty of arc signature recognition in both time and frequency domain. An example of FFT analysis for baseline noise and arc signature analysis is given in Figure 4. From the picture, the arc signal is easily disguised by the existence of background noise comprised of the inverter switching noise and the harmonics. Therefore the reliable differentiation between arc fault and normal switching event need to be solved in the development of AFD/AFCI.

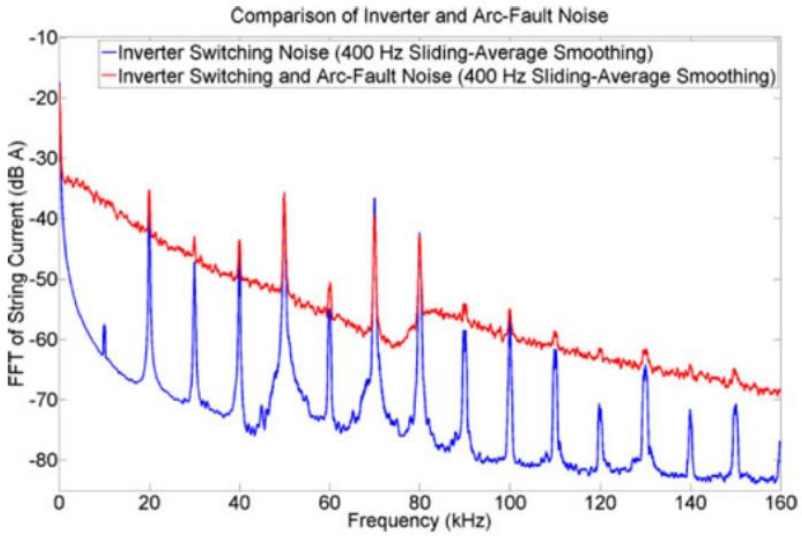

Figure 4 Comparison of inverter and arc fault noises taken from [11]

1.3 Wavelet based arc fault detection algorithm

Wavelet transform (WT), an emerging multiresolution frequency analysis method, is studied in recent years and applied in the power system analysis such as disturbances study, power measurement, harmonic and power quality analysis, etc [39-46]. Arc fault detection is one of the major application [47].

WT based detection algorithm is developed in recent years [48-50]. It decomposes a signal using a wavelet package and the base wavelet for the decomposition is an oscillating wave with finite energy. After different scaling and shifting, the non-periodic base wavelet can form daughter wavelets which contain adjustable magnitude and length [51]. Therefore WT performs better characterizing non-periodic signal like abrupt changes in current when arc fault happens. The graphical representation of WT process is given in Figure 5. Furthermore, the computational complexity of WT is on the order of N which

is no more than the computational stress of FFT. Also, since the multi-resolution analysis is applied to different frequency band, the complexity of the algorithm can be modified to suit the requirement.

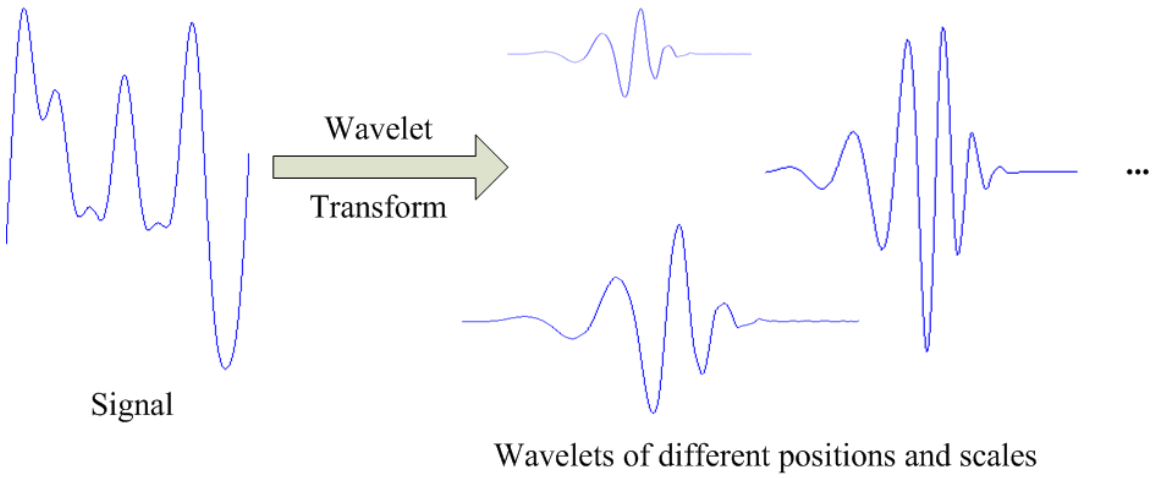

Figure 5 Graphical explanation of Wavelet Transform

A comparison of the time and frequency resolution between FT and WT is shown in Figure 6. As analyzed before, FT has invariable time and frequency resolution once the window size is fixed. However for WT, the frequency domain resolution is finer at low frequency where the time domain localization is not as important so that the low frequency content can be differentiated clearly. For high frequency band where signal changes rapidly, time domain resolution is kept high so no high frequency feature can be localized accurately. This is realized by multiple levels of decomposition, each level doubles the

frequency resolution and halves the time domain resolution compared to the one previous level and it's suitable for analyzing the non-stationary signal.

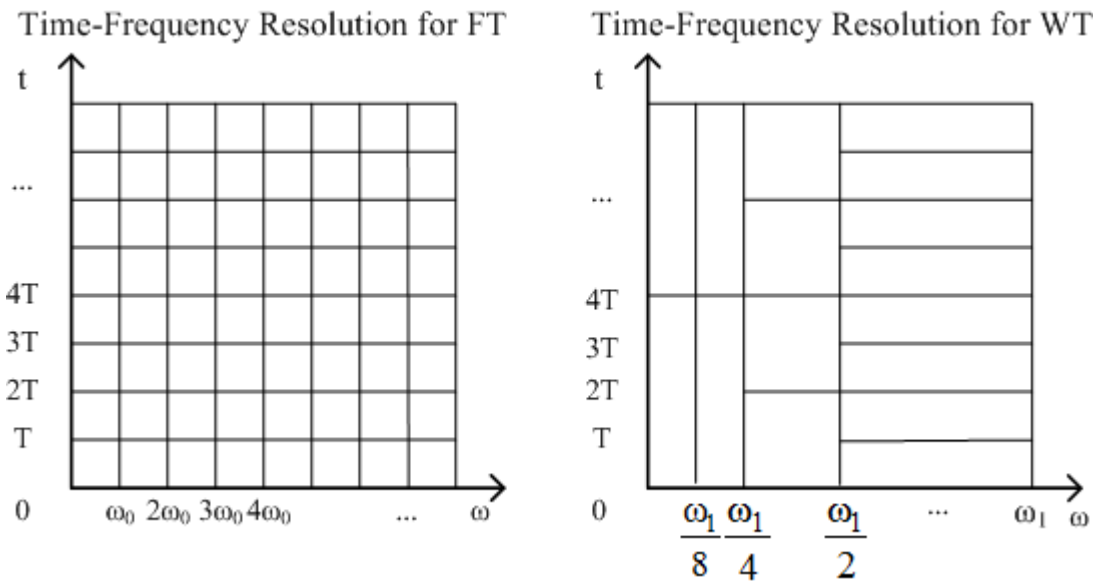

Figure 6 Time and frequency resolution comparison between FT and WT

1.4 Research objective

The challenge of this research is the realization of WT based real-time arc detection of the PV DC systems. Though the utilization of wavelet in the arc fault detection has been studied in the literature, little information about the implementation on hardware and details of the real-time arc detection test is given. There are several concerns involved and questions to be answered. On the hardware side, is there any hardware specification or requirements to meet in order to realize WT based algorithm and should any preprocessing be done to the arc signal; on the software side, how to implement the WT algorithm on

the detection hardware; and on the real-time test, how is arc signal obtained and provided to the detection system, etc.

The research mainly contains three topics. First, investigation of suitable hardware for arc signal acquisition; second, generation of steady and easily replicable arc signal on the PV DC systems; third, realization of WT based detection algorithm and demonstration of its rationality through real-time tests, then compare and analyze the difference of FT and WT based detection technique.

1.5 Thesis outline

This thesis contains six sections.

Section 1 gives a brief introduction of this project. The necessity of arc fault detection is clarified through the description of arc fault phenomenon on the PV DC systems. The incompetence of the prevailing FT based detection method and the hardly recognizable nature of arc signature makes the reliable arc fault detection on PV systems a challenge. As an alternative, WT is considered as a better solution. The research objective is to realize the WT based detection technique and justify it through real-time arc detection tests.

Section 2 talks about the theoretical study related to arc detection using WT based detection technique. WT theory and its implementation in discrete system is illustrated. Also, the concept of Arc-Signal-Noise-Ratio (ASNR) is introduced to better characterize the power of the arc signal. Theoretical analysis of arc signal comparing FT and WT detection technique is given.

Section 3 describes the construction of arc fault testbed and technique to reproduce the arc signal on PV system. With the assistance of automation software, the testbed is calibrated and the unity gain system is built. Arc signal is reproduced through the graphical user interface (GUI) through the arc fault testbed.

Section 4 illustrates the detection hardware including its structure and processing capability. Different coding technique are tested and the one best suits the hardware is applied to program WT algorithm. After upgrade of processor, 2-levels wavelet decomposition with 200kHz sampling frequency is realized.

Section 5 shows the real-time detection result. Threshold setting for the arc detection is conducted through the simulation process in MATLAB. The real-time detection result utilizing FT and WT based algorithm are compared and further discussed for both synthesized arc signal and real PV arc signal.

Section 6 concludes the work and gives some suggestion for the future work.

2. THEORETICAL STUDY

2.1 Wavelet Theory

Wavelet is a mathematical tool for signal analysis first introduced in 1909 and gradually developed since the 1970s. A wavelet is a short duration wave, and the sufficient and necessary condition for wavelet is it has to be oscillatory and decays to zero quickly, with a zero average value [52]. Wavelet transform is a multi-resolution analysis (MRA) method to analyze transient signals which provides multiple resolution in both time and frequency domain.[53]. It decomposes a signal into different scales based on the prototype function "mother wavelet". The mother wavelet can transform into more wavelets through various scaling and shifting process, and the signal can be represented as the superimposition of a set of wavelets. The auxiliary scaling function is also called the "father wavelet". While characterizing transient signals, WT can accurately reproduce the signal with less components compared to FT based analysis [54].

Corresponding to the mother wavelets which determines the shape of the components in the decomposition, the dilated and translated version is called daughter wavelets. The dilations and translations of the wavelet are orthogonal basis of $L^2(R)$ [55]. The continuous wavelet function can be expressed as:

$$\psi_{a,b}(t) = |a|^{-1/2}\,\psi\left(\frac{t-b}{a}\right) : a \in R, b \in R \tag{3}$$

In the equation, *a* represents the scale parameter related to frequency and *b* represents the dilation parameter related to time or position. Result of the continuous wavelet transform (CWT) is expressed as:

$$X_{CWT}(a,b) = \int x(t)\psi_{a,b}(t)dt \tag{4}$$

In discrete system, the scaling parameter $a = 2^p$ and the dilation parameter $b = q2^p$ where p and q are integers chosen according to the analysis requirement. Therefore the discrete wavelet transform can be expressed as:

$$\psi_{p,q}(n) = 2^{-p/2}\psi(2^{-p}n - q) \tag{5}$$

and the signal to be analyzed using discrete wavelet transform (DWT) can be represented by:

$$x(n) = \sum_p \sum_q c_{p,q}\psi_{p,q}(n) \tag{6}$$

where $c_{p,q}$ is the inner product of the signal and the corresponding wavelet.

The result of wavelet decomposition at each level has two parts. One called 'approximation' which contains low frequency content representing the sketch of the waveform to be analyzed, the other part is called 'detail' which contains high frequency feature on top of the waveform sketch. After several levels of decomposition, the waveform can be expressed as the superimposition of approximation and detail at different frequency band as shown in equation:

$$x(n) = \sum_q a_{p0,q}\psi_{p0,q}(n) + \sum_q \sum_{p=p0}^{\infty} d_{p,q}\psi_{p,q}(n) \tag{7}$$

The coefficient of $a_{j0,k}$ and $d_{j,k}$ are developed using quadrature mirror filters (QMF). The QMF divides the frequency band evenly into two parts: highpass and lowpass [56]. The high pass filter in the QMF is related to the mother wavelet and the lowpass filter is related to the scaling function. In another way, the approximation is obtained from

the lowpass filter and detail is computed through the highpass filter. The approximation can be used in further decomposition to extract more features. Figure 7 shows the dyadic tree filter bank structure to implement the DWT. As it is shown in the figure, each level halves the frequency analysis bandwidth compared to the previous level of decomposition and the approximation and detail are obtained through the QMF.

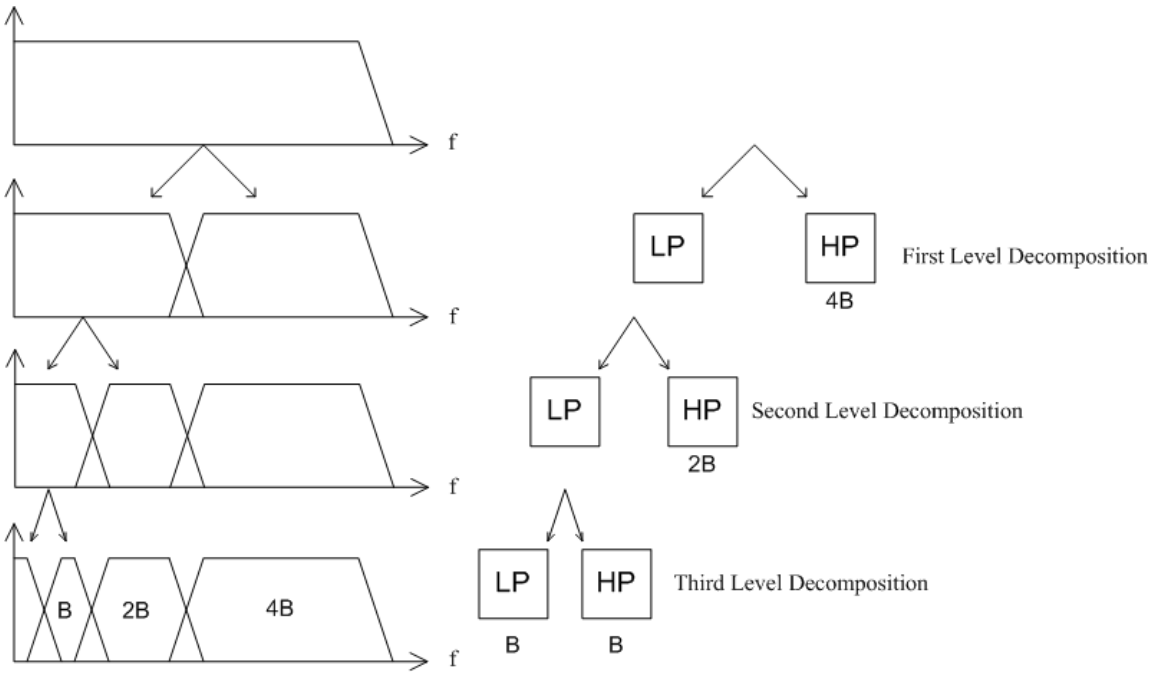

Figure 7 Implementation of DWT through quadrature mirror filter in dyadic tree structure

There are different types of wavelets to suit various application, such as Haar (h), Daubechies (db), Coiflet (c), and Symmlet (s). In the arc fault detection, Daubechies family wavelet is applied. The number following with ‘db’ represents the number of vanishing moment of a wavelet [57] defined in equation (8):

$$\int x^{\mu}\psi(t)dt = 0 \tag{8}$$

The more vanishing moment a wavelet has, the more complex a wavelet is and the better such wavelet characterizes the oscillating nature of the transient signal. For example, Figure 8 gives the scaling function and wavelet function for db3, db9, and db19. The wavelet becomes finer with the increment of vanishing moments.

In DWT, the number of vanishing moments is characterized by the length of filter coefficient. The coefficient length is proportional to the analysis performance of wavelet, the longer the better. Figure 9 shows the lowpass and highpass coefficient for db3, db9, and db19.

In the frequency domain, filter length is proportional to the analysis performance. As it's shown in Figure 10, frequency transition is sharper with the increment of number of filter coefficient and the gain at both passband and stopband is flatter [35]. In other words, the results of lowpass and highpass filter are more accurate.

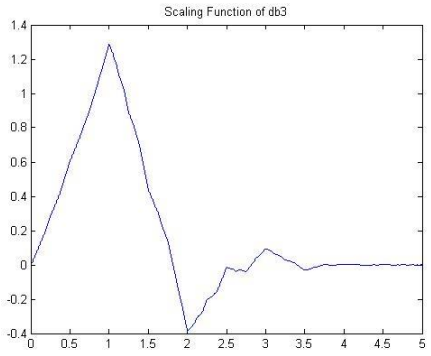

(a). Scaling function of db3

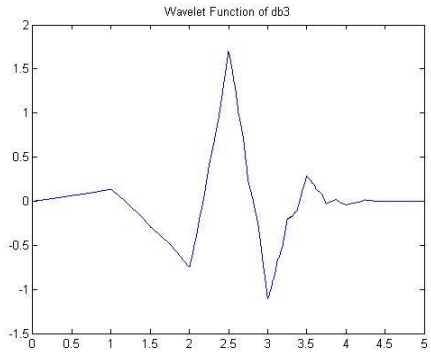

(b). Wavelet function of db3

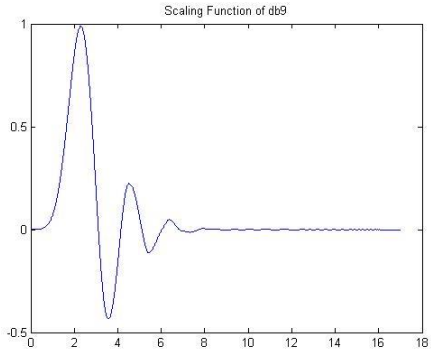

(c). Scaling function of db9

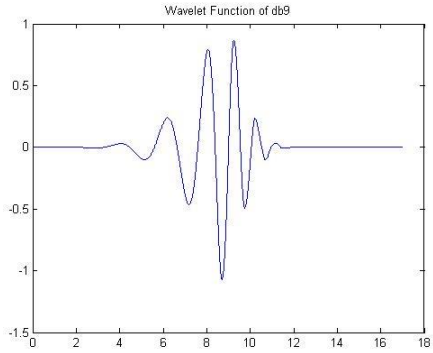

(d). Wavelet function of db9

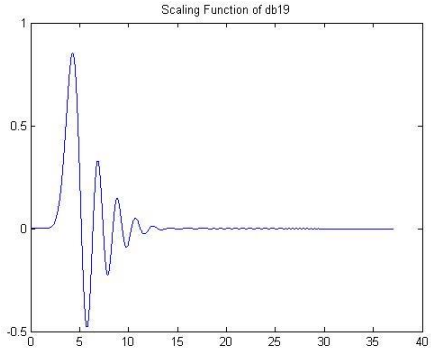

(e). Scaling function of db19

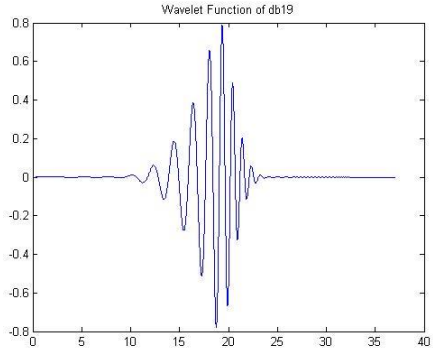

(f). Wavelet function of db19

Figure 8 Scaling and wavelet function of db3, db9, and db19

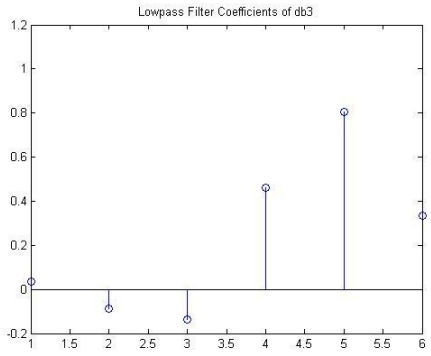

(a). Lowpass coefficient of db3

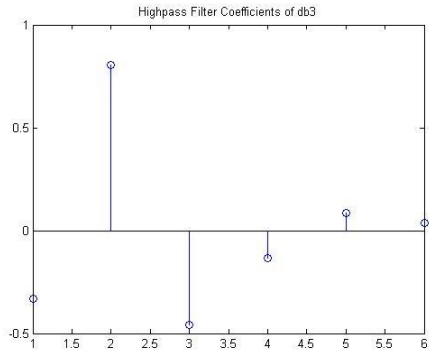

(b). Highpass coefficient of db3

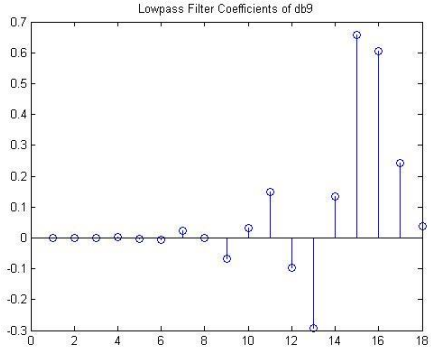

(c). Lowpass coefficient of db9

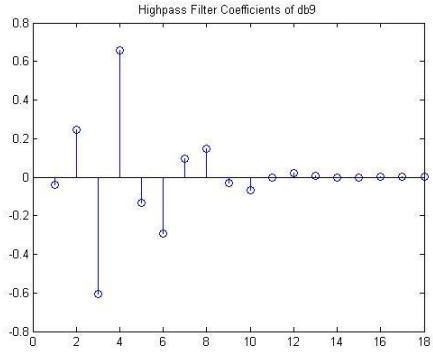

(d). Highpass coefficient of db9

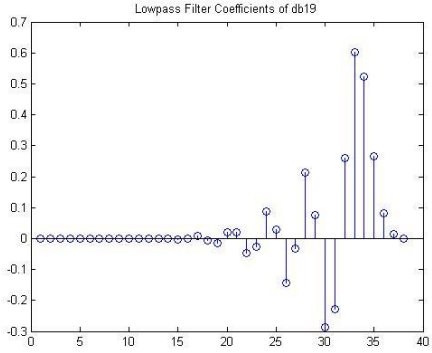

(e). Lowpass coefficient of db19

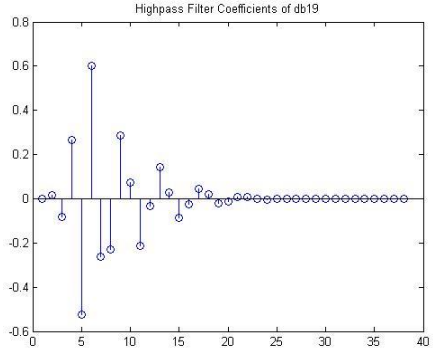

(f). Highpass coefficient of db19

Figure 9 Lowpass and highpass filter for db3, db9, and db19

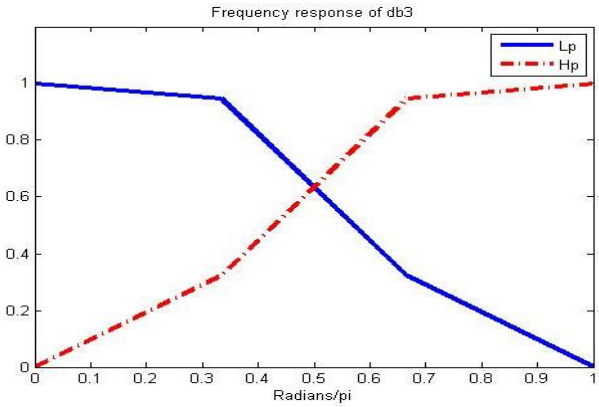

(a) Frequency response of db3 wavelet

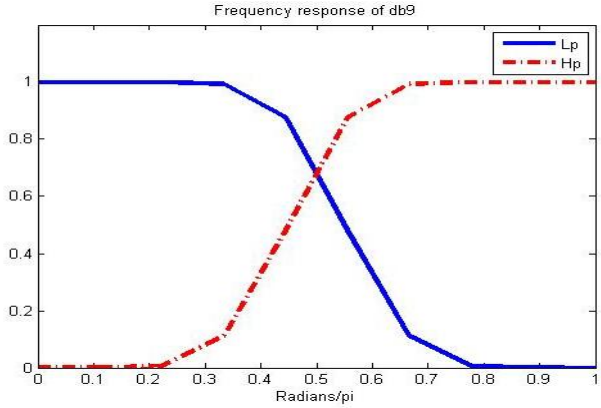

(b) Frequency response of db9 wavelet

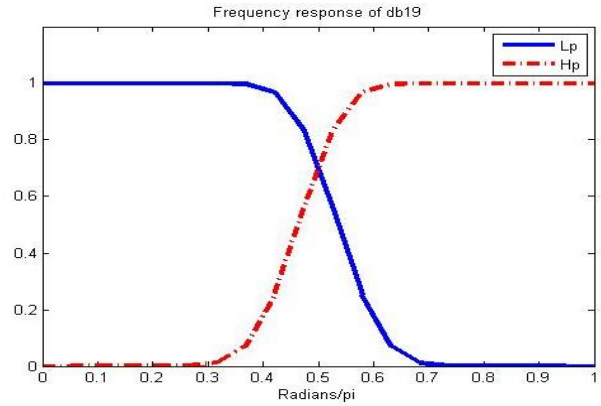

(c) Frequency response of db19 wavelet

Figure 10 Frequency response of filter banks using db3, db9, and db19 taken from [35]

2.2 Arc-Signal-Noise-Ratio (ASNR)

Grid-tied PV systems are connected with solar inverters, and the switching action generates high frequency noises. It's crucial for the detector and detection algorithm to successfully distinguish the background noise and the erratic feature of arcing event. In the literature, researchers used to study the characteristic of arc signal through arc generators connected to PV systems and create the arc signal by separating two opposing electrodes [58-62]. However the power of PV arc signal is uncontrollable, also the frequency characteristic measured from one single PV system may not be universally representative.

To overcome this complication, a concept called Arc-Signal-Noise-Ratio (ASNR) is introduced. It describes arc signal by the ratio of power of the arc signal to power of the inverter noise [38]. By adapting different ASNR, arc signal can be synthesized using inverter noise measured from PV systems and arc signature obtained from arc generators. This method endows researchers to have better convenience and flexibility by composing arc signal using various inverter noise and arc event library in different combination, and the power of the arc signal is adjustable and controllable. The definition of ASNR is given in the equation (9):

$$ASNR = \frac{P_{arc}}{P_{noise}} \tag{9}$$

In the equation, $P_{arc/noise}$ is the average power of the recorded arc or noise signal, and it's computed through equation (10):

$$P_{arc/noise} = \frac{\sum M^2}{L} \tag{10}$$

Here M stands for the signal magnitude and L stands for the length or in other words the total number of points in the recording frame. Power of the arc signal is measured from the duration when arc signal remains relatively. The amplitude of the arc signal is scaled according to the ASNR researchers set:

$$Arc_{scaled} = Arc_{recorded} \times \sqrt{\frac{ASNR_{set}}{ASNR_{actual}}} \tag{11}$$

Rather than using simple amplitude superimposition of the arc and noise signal, the synthesized waveform is composed of inverter noise and scaled arc signal:

$$Arc_{syn} = Inv + Arc_{scaled} \tag{12}$$

ASNR equaling to 0.01, 0.1 and 1 are chosen as representative of small, medium, and large arc power level and are studied throughout the study. It's also worth mentioning that the original inverter noise used in the project only has 0.05s duration while the recorded arc signal has 1s length. Therefore the inverter noise is analyzed using FFT and reconstructed through IFFT technique so it's extended in time domain to a desirable length.

Figure 11 shows the original signal and synthesized arc signal. From the figure, arc signal becomes less observable with the decrement of ASNR.

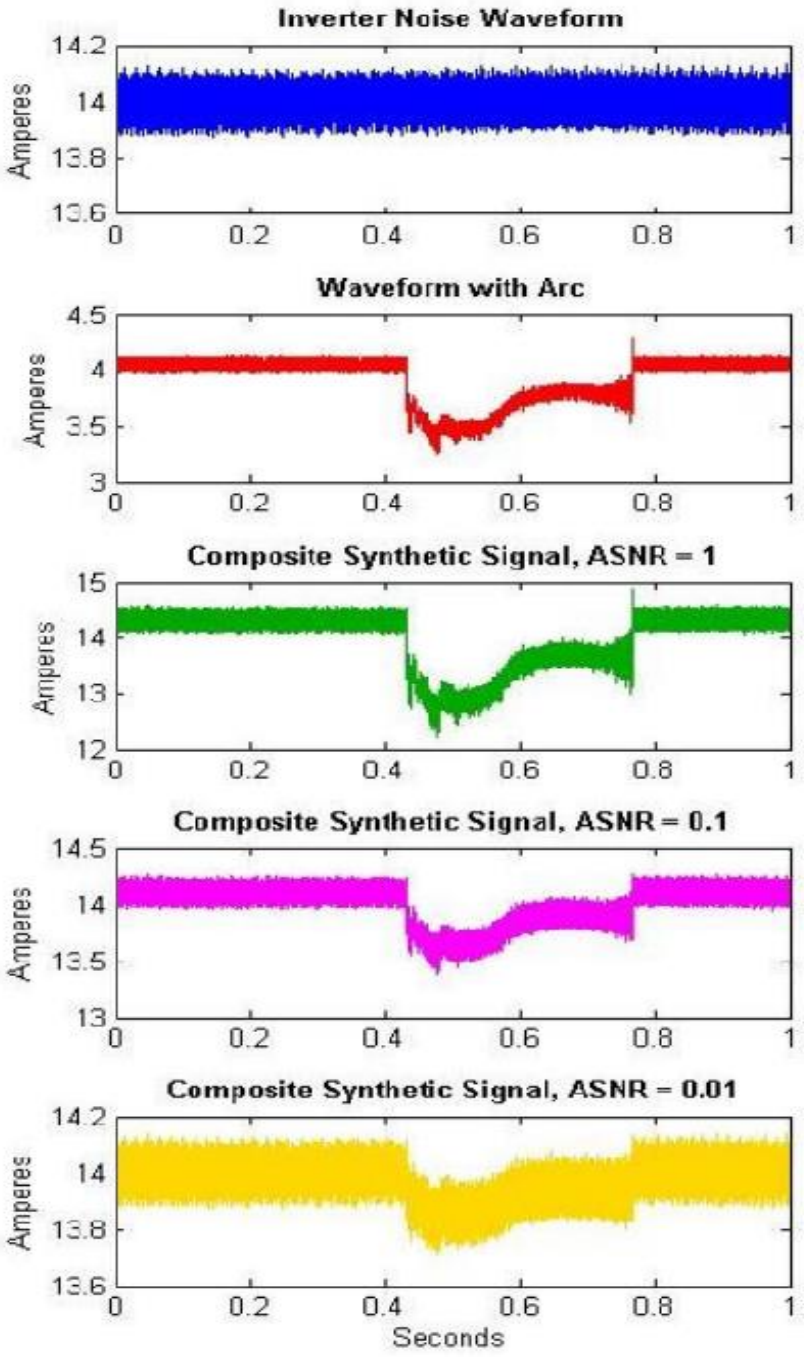

Figure 11 Synthesized arc signal for ASNR=1, 0.1, and 0.01 taken from [38]

2.3 Theoretical analysis of FFT vs. WT

As mentioned before, theoretically FFT is less capable to analyze frequency content at variable resolution and to localize the abnormal event however case study is needed to prove the ineffectiveness of FFT base detection algorithm. Therefore the composite arc signal with 1s duration are studied to compare FFT and WT algorithm.

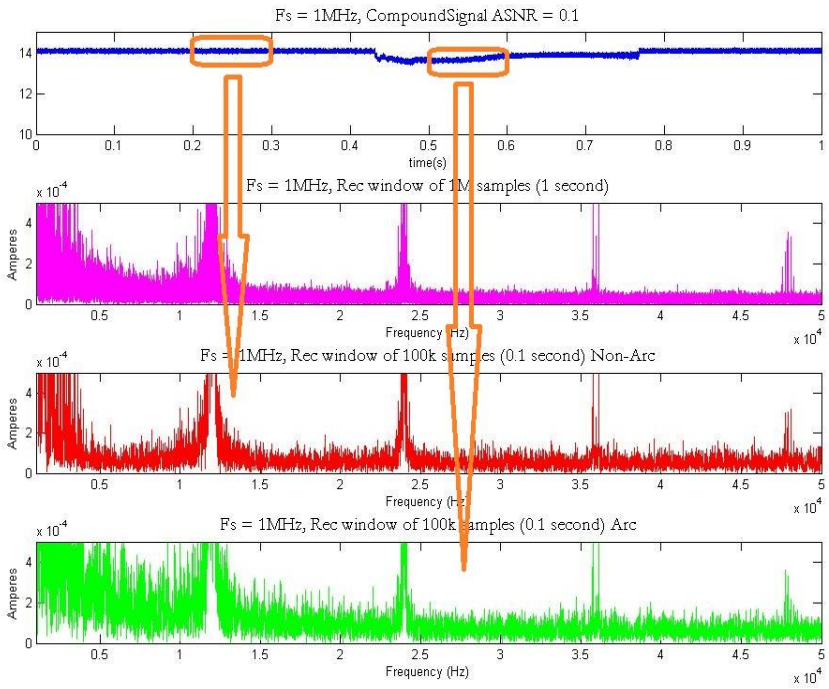

Figure 12 FFT analysis of composite arc signal (Fs=1MHz, ASNR=0.1) taken from [35]: entire frame (magenta), non-arcing duration (red), and arcing duration (green)

FFT analysis to a composite arc signal with ASNR of 0.1 is conducted in MATLAB. The synthesized signal is obtained with 1MHz sampling rate and the analysis result is shown in Figure 12. In the figure, FFT analysis for the entire 1s frame (magenta), non-arcing frame (red), and arcing frame (green) show no clear difference indicating the impossibility to differentiate arcing from non-arcing state.

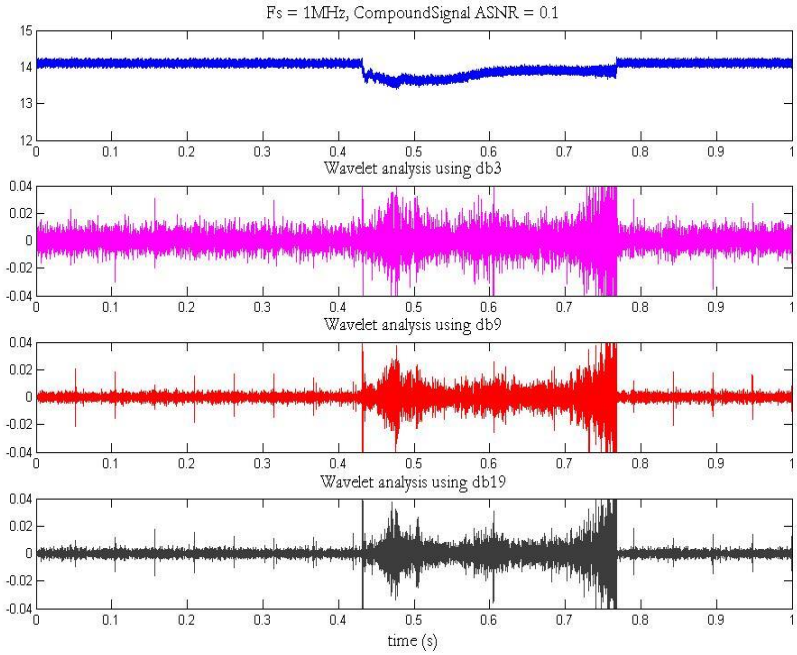

Figure 13 WT analysis of composite arc signal (Fs=1MHz, ASNR=0.1) taken from [35]: db3 (magenta), db9 (red), and db19 (black)

As a comparison, WT analysis result is given in Figure 13. Shown in the figure is the detail of 7th level decomposition, covering frequency band of 3.9kHz - 7.8kHz. Increment of the signal amplitude differentiates arcing from non-arcing state.

Decomposition using db3 (magenta), db9 (red), and db19 (black) all show the clear feature of initiation and extinction of the arc signature. The output of WT for each frequency band is time domain signal, enabling good temporal event localization.

Another observation from Figure 13 is the accuracy of analysis. Finer coefficients increases the observable feature to distinguish arcing from non-arcing however the performance improvement becomes less obvious from db9 to db19. Therefore it may not be necessary to utilize the high performance filter for the sake of reducing the amount of computation and saving hardware resources usage.

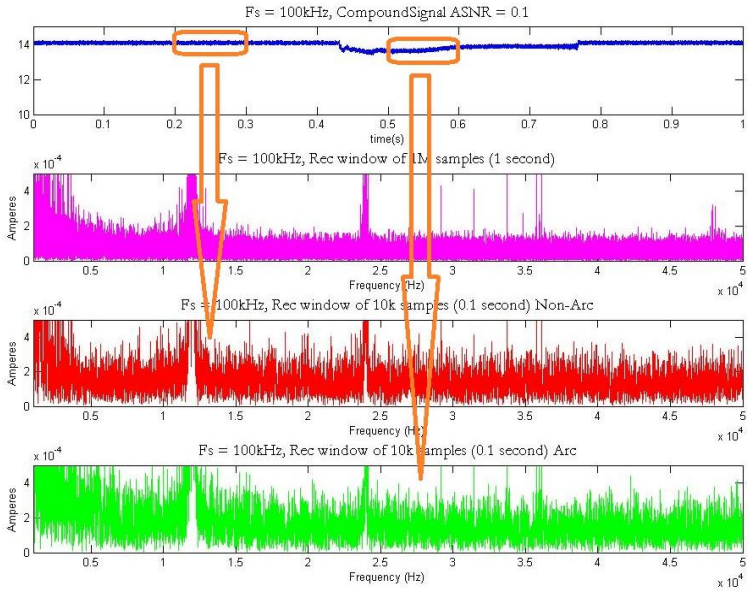

Figure 14 FFT analysis of composite arc signal (Fs= 1 MHz, ASNR= 0.1) taken from [35]: entire frame (magenta), non-arcing duration (red), and arcing duration (green)

To further explore the influence from sampling rate to the analysis result, the composite signal is downsampled to reach sampling rate at 100kHz. FFT result is given in Figure 14, with same data frame applied as the input. With fewer sample points, even less frequency feature can be extracted due to the reduction of frequency resolution. No different conclusion can be drawn comparing the arcing and non-arcing characteristic, and furthermore, the discrepancy between these two states becomes vaguer.

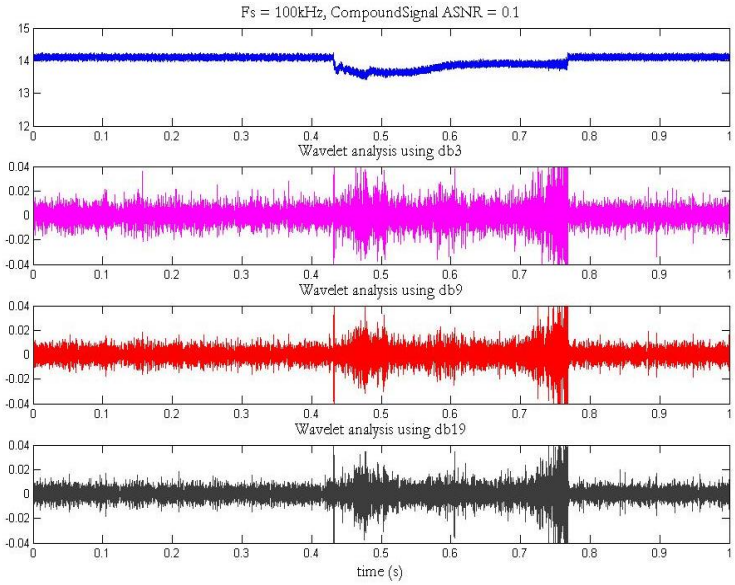

Figure 15 WT analysis of composite arc signal (Fs=100 kHz, ASNR= 0.1) taken from [35]: db3 (magenta), db9 (red), and db19 (black)

Shown in Figure 15, by utilizing WT, even though the presence of arc is not as obvious as 1MHz sampling frequency, there's enough feature to determine the occurrence

of arc event. However with the reduction of sampling frequency, performance improvement after using advanced filter also becomes less noticeable.

From the theoretical analysis comparing FFT and WT, sampling rate has significant impact on the analysis result for both techniques. However even with high rate data, FFT is not capable to differentiate arcing event from non-arcing state, nor to say the temporal localization of where the arc occurs within the data frame. WT by contrast, exhibit the distinction of current amplitude between the two status at certain sub-band and enough feature is kept to discriminate the arc event even with reduced sampling frequency as low as 100kHz. Therefore from the theoretical study utilizing real arc data, the preliminary conclusion that WT has better performance detecting the arc signal can be drawn.

3. ARC DETECTION TESTBED

3.1 Structure of the testbed

Detection of arc in a real PV system is crucial but challenging as the arc signal might remain sustained but undetected because of the intrinsic high frequency signal in PV systems. The high frequency noise is part of the nature of PV arc signal but impossible to be duplicated under lab condition. A solution to such difficulty is to reproduce a pre-recorded arc signals including the high frequency feature using a high fidelity testbed. Such testbed should have the capability to reproduce an analog arc signal in the same power level with the recorded arc. The purpose of the high fidelity testbed is to recreate the steady arc signal with true arc characteristic with convenience and efficiency.

Structure of the testbed is shown in Figure 16. The testbed is comprised of a computer, a digital to analog converter (DAC), a power amplifier, a resistive load, and an oscilloscope. The computer stores the recorded arc signals, and the synthesized signal is applied in the study. This composite signal is derived through inverter noise obtained from lab generated arc signature and operating PV systems. A key step in the reproduction process is the conversion from digitized signal back to analog voltage signal through DAC device. Note that the recorded information is the arc current which is not the same with the output voltage of DAC device. Considering the incapability of DAC device to output enough current as recorded arc current, the power amplifier is connected to the output of the DAC. The amplifier provides extra power and amplifies the output voltage so the resistive load in series with the output port can draw enough current. In this way, the

recreated signal contains the same power with pre-recorded arc current and the determination can be made based on the analysis of the output current of the testbed.

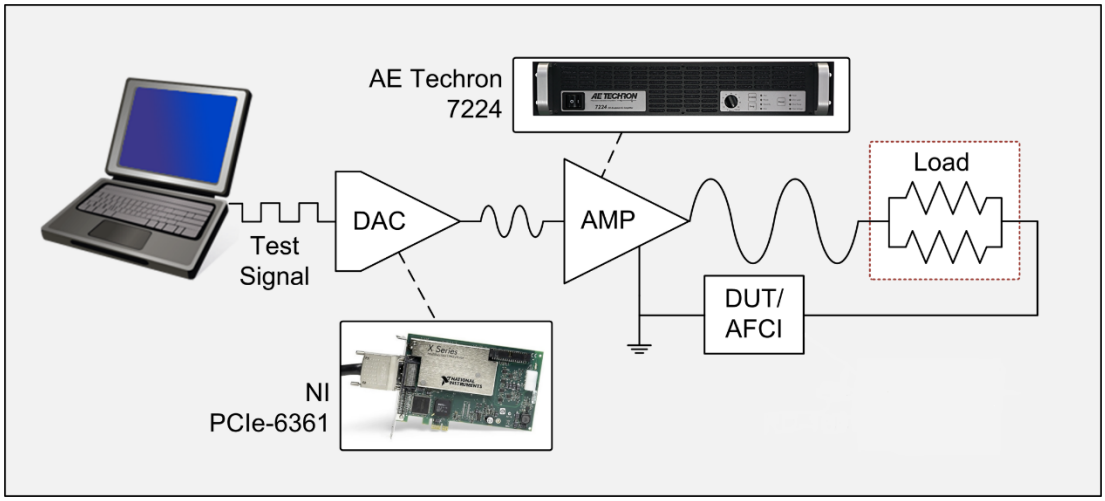

Figure 16 Structure of the high fidelity testbed

Several concerns have to be considered for the equipment selection. First, the output rate of DAC should be high enough to keep the real frequency characteristic. If the sampling rate of DAC device isn't high enough, the recorded signal might need to be downsampled to suit the capability of DAC device and the high frequency feature of the arc signal could be missed. Also it should be noted if the DAC is equipped with lowpass filter at the output. For DAC devices which only sample and hold the output voltage potential without lowpass filtering, the frequency characteristic might be changed as well. Second, there should be enough data resolution for the DAC to represent the true frequency feature of arc signal such as small magnitude high frequency signal. Moreover, the power amplifier should be able to provide enough power to reproduce the arc signal.

It’s also necessary to check if the power amplifier has DC voltage output ability and whether the output voltage required to generate the arc current falls within its output range. Further the bandwidth should be higher than the frequency band of interests for arc signals, and no distortion should be introduced to this frequency spectrum. Finally, the power rating of the resistive load should be higher than the power of the arc signal that the load won’t be damaged during the reproduction.

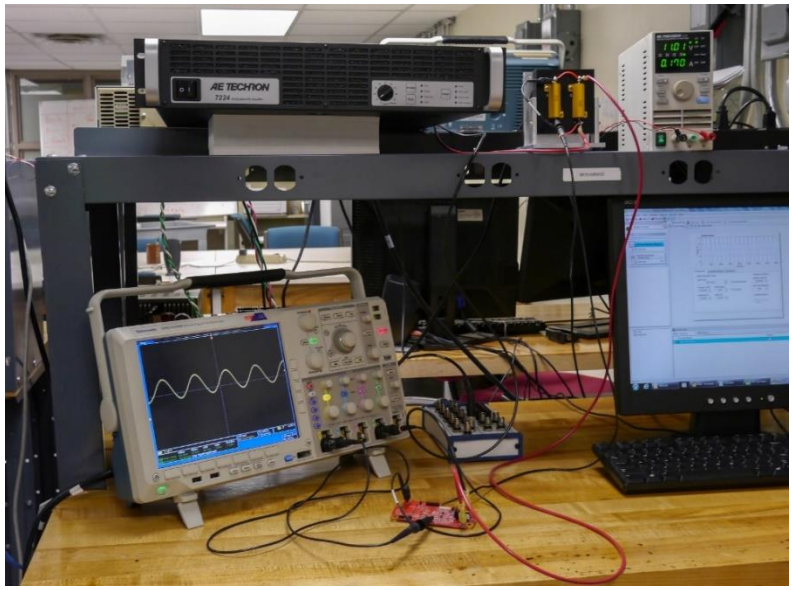

Figure 17 Picture of the high fidelity testbed

With aforementioned consideration, the DAC and power amplifier equipment selected in this testbed are the National instruments PCIe-6361 and the AE Techron 7224. The NI PCIe-6361 permit 16-bit sampling with up to 2.86MS/s output rate, the output voltage range is (-10, +10) V. The AE Techron 7224 can amplify the voltage to up to 140V with max 1.2kW output power. Most importantly, these two devices have constant gain within the frequency band of our interests, hence the frequency characteristic of the arc signal can be kept accurate. Figure 17 shows the picture of the testbed. The oscilloscope is used to assist monitoring signals.

3.2 Calibration using automation program

Arc signal contains wide spectrum, and our previous research focused on the frequency content below 100kHz. A precise calibration is needed to validate the invariant passband gain in the frequency response of the testbed. Among all equipment selected, no distortion is expected at any stage of the reproduction procedure.

The idea of the calibration is to provide digital sine waves input with different frequencies and perform a frequency sweep covering the frequency band of interests. A frequency response plot of the testbed can be made after the output magnitude and phase shift are measured. Instead of the absolute value of the output waveforms, the variation between different frequencies is where the attention should be paid. The magnitude is obtained from the measurement function on the oscilloscope while the phase shift is computed through the time difference between zero crossing points of input and output waveform of the testbed.

The Data Acquisition Toolbox in MATLAB is used for the interaction between computer and hardware. It contains the driver information of data acquisition equipment like ADC, DAC, function generator, and oscilloscope, and establishes the connection between data acquisition devices. With the assistance of the toolbox, a hardware object can be configured and the device can be manipulated from the computer. In the calibration, the digital sine waves from 10kHz to 160kHz with 10kHz interval are generated with a sampling frequency of 2.5MHz. The NI PCIe-6361 is not equipped with a lowpass filter so the sampling frequency is set to be much higher than the frequency of the sine waves in order to smooth the output. For each single frequency, the input sine wave is sent and buffered to the DAC. The sine wave is reproduced and measured once the replay command is executed in MATLAB. The frequency sweep is accomplished through repeating the steps for all frequencies in a 'for' loop.

The frequency sweep plot obtained from the calibration is shown in Figure 18. Three sweep results are given as examples. In the plot, the magnitude of output voltage of all frequencies are unified to 10 kHz in order to show the tendency of variation. From this plot, unified magnitude of output voltage swings between (0.96, 1.01) and the phase shift of the three tests has the same linearity. Considering the possible measurement error from the oscilloscope, the testbed is believed to have an invariant magnitude gain and constant time delay within the frequency band of interests. Therefore, the testbed should have high fidelity reproduction capability- no distortion is introduced while reproducing the arc signals.

An automation software is developed using MATLAB script in order to accelerate the calibration and reproduction. The program consists of 5 parts:

1.) configure the hardware object and the device connection with the computer;
2.) configure the measurement and signal acquiring property of the oscilloscope;
3.) buffer the digital signal into the equipment;
4.) play the buffered data;
5.) record waveform and save recreated data from the oscilloscope, and transfer data back to the computer for further processing and analysis in MATLAB.

All the data and files are transferred directly to the local disk of computer through Ethernet cable instead of manually operated flash drive, and they're also saved as a variable in the MATLAB workspace. Once the data has been buffered into the hardware, the whole process can be easily repeated by executing replay command again. The predominant merit of the program is the automation of measurement and hardware interaction through MATLAB program. The steps of reproduction are executed sequentially by software and the possible error from incorrect test procedure can be avoided. Moreover, the automation substantially improves the efficiency by eliminating unnecessary manual operations.

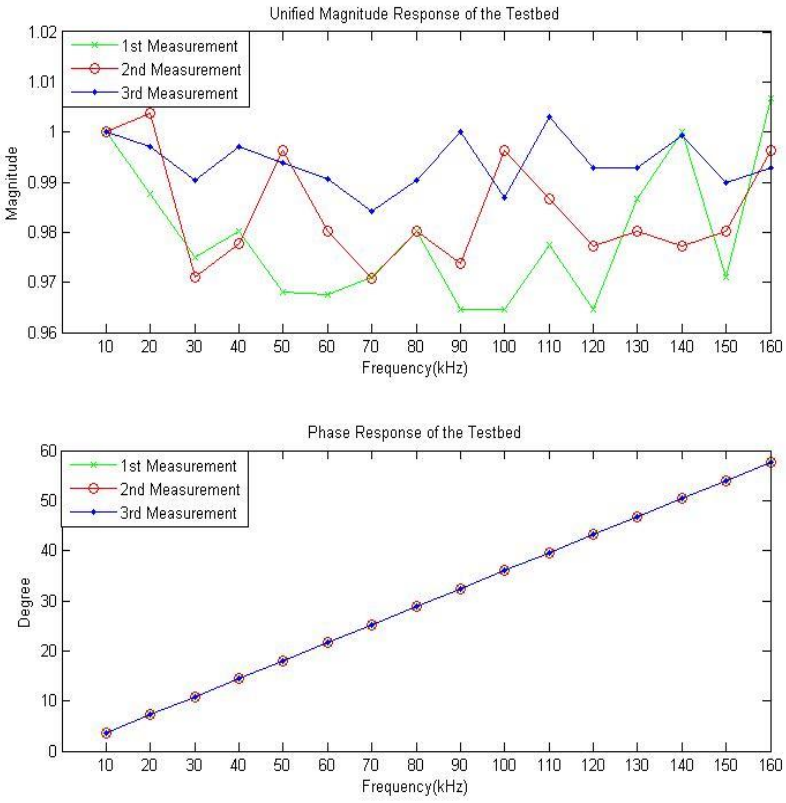

Figure 18 Three examples of calibration test

3.3 Construction of unity gain system

Given the fact the testbed has invariant frequency response within frequency band of interests, one more step is needed for the faithful reproduction of the arc signal. A hand-operated rotary knob determines the amplification factor of the power amplifier, and it needs to be tuned to the unity gain position, that being said the output power of the testbed should be the same as the arc signal.

For highly unregulated signals like arcs, it's difficult to define a representative frame of wave and determine the magnitude of the signal based on that certain duration.

Therefore, average power of a data frame introduced earlier is used for evaluation. The average power of the current signal is compared between the original and the reproduced arc.

The original recorded arc data has 1M sample points with 1MS/s sampling rate. In the experiment, DC offset of the arc signal is removed in MATLAB to preserve the high frequency characteristic, otherwise the minute high frequency signal could be invisible on the oscilloscope. The recreated signal is recorded through a current probe and imported to MATLAB through Ethernet cable, hence the average signal power can easily be derived. The amplification factor on the power amplifier can only be modified through a rotary knob, therefore it's almost impossible to find the perfect unity gain position where average power of original and reproduced arc are exactly the same. Table 1 listed the average power of the synthesized signal at ASNR = 0.01, 0.1 and 1 at same position closest to the perfect unity gain position through manual adjustment.

It can be observed from the table, the average power of the 1s frame containing 1M sample points are almost the same for original and reproduced signal, and the unity gain position found applies to all different ASNR. Therefore the unity gain system is irrelevant to the different input signal of the testbed.

Table 1 Average power of original signal on testbed vs. composite in MATLAB

Average Signal Power	ASNR=1	ASNR=0.1	ASNR=0.01
Original signal	1.0661	0.1133	0.0194
Composite signal	1.0476	0.1122	0.0188

Figure 19 and Figure 20 shows the example of original and recreated arc signal for ASNR= 0.1. From the comparison of this two figure, the sketch of the waveform are accurately replicated including the abrupt drops and raises. Some high frequency spikes might look different, however this is tolerable as long as the power of the reproduced signal is the same as the original arc signal.

Combining the calibration of frequency response of the testbed and construction of unity gain system using average power comparison, the accuracy of the testbed is guaranteed. With the synthesized arc signal reproduced from such high fidelity testbed, not only the inverter noise characteristic is preserved and displayed under lab condition, but also the efficiency of arc fault study is enhanced significantly.

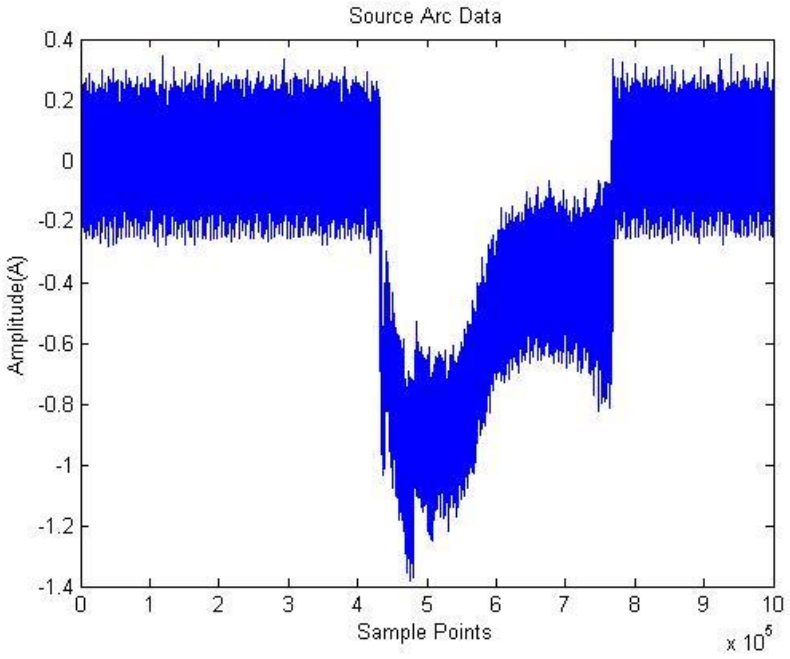

Figure 19 Original synthesized arc signal (ASNR= 0.1)

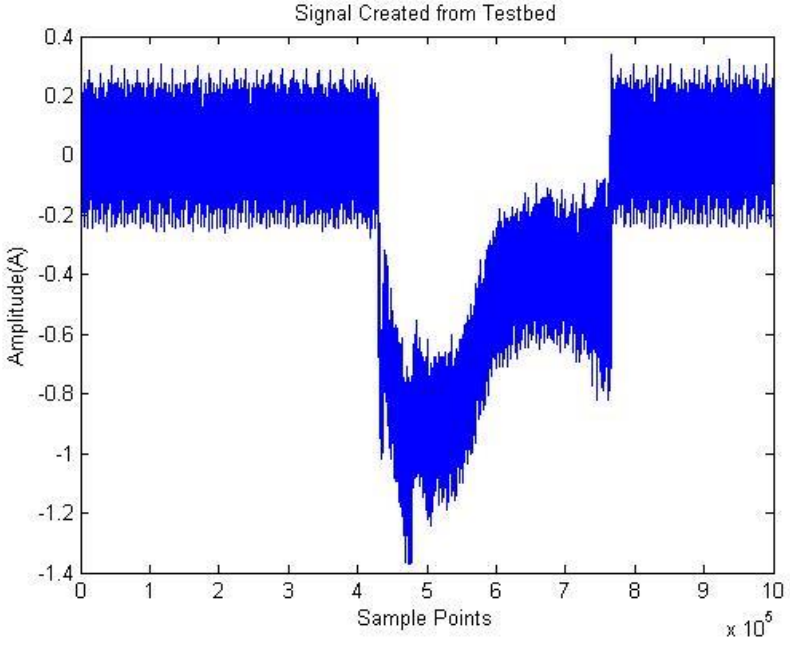

Figure 20 Reproduced synthesized arc signal (ASNR= 0.1)

3.4 Graphical User Interface (GUI)

Considering the possible large amount of arc and inverter data and the different combination possibility, a graphical user interface (GUI) is developed in MATLAB using its graphical user interface development environment (GUIDE). The purpose of the GUI is to expedite the signal synthesis and real-time control of the composite arc signal. It's desired to encapsulate different function blocks in the arc fault study into one panel so that researchers won't be bothered to know the details of each function nor do much unnecessary work like calling functions and saving files by themselves.

The GUI panel is shown in Figure 21. The GUI has four function classification: signal synthesis, analysis, file management and real time reproduction. User can select arc and inverter data in the pop-up window after clicking on the data selection button. The arc signal will be synthesized and plotted according to the ASNR input to the textbox. After the arc signal is composed, user can do FFT analysis on arc, inverter, and synthesized data based on the sampling rate specified in another textbox. Both synthesized waveform and analysis result can be saved to the local file directory using buttons provided in file control. Then the composite arc signal can be replayed and recorded again using real time control buttons. The hardware connection between devices and computer are established when clicking the real time control button. The aforementioned function such as buffering data to the DAC device, replaying data, and saving both waveform and screen shots can all be accomplished using the real time control functions. Another feature of the GUI is it keeps a copy of all internal variables created like the synthesized arc data, FFT analysis result, or recorded waveform from the oscilloscope in the MATLAB base workspace. If not

enough analysis function is provided, user can continue their research by programming their own functions in MATLAB using these variables saved in the base workspace. It's also possible to compile the GUI into a standalone executable file that can run outside MATLAB using a toolbox called MATLAB Compiler.

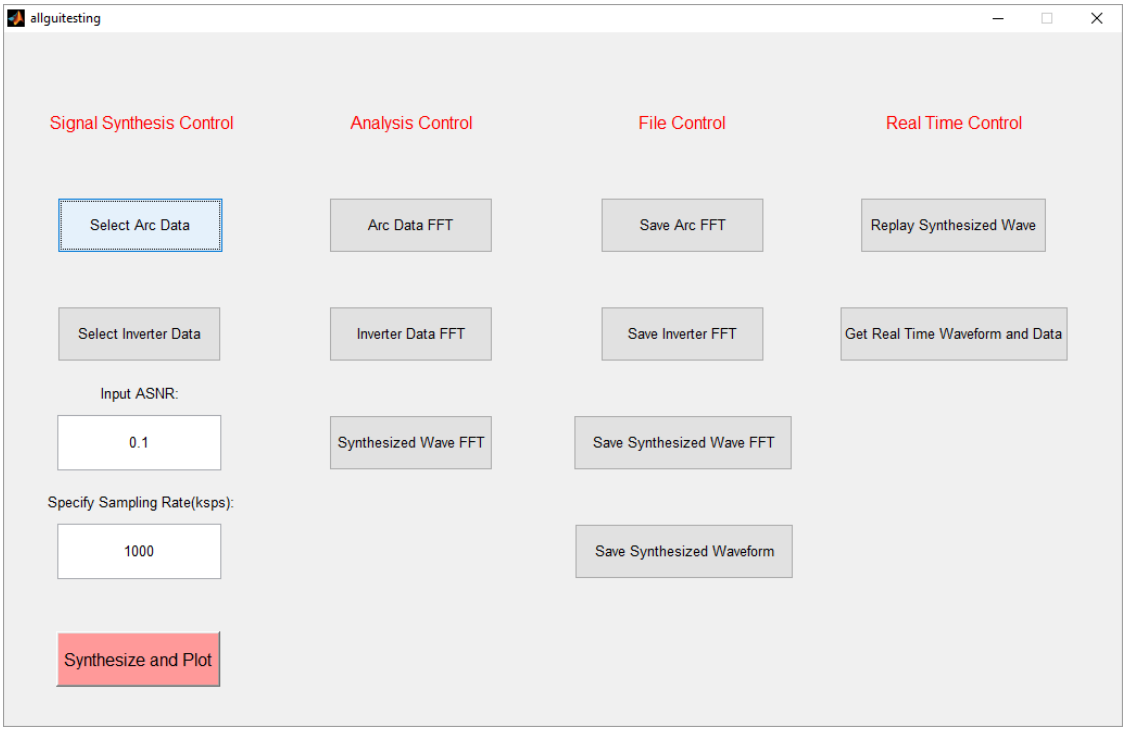

Figure 21 Arc study GUI

4. DETECTION HARDWARE

4.1 DC arc detector- RD-195

In the arc detection, the detection hardware determines how the arc signal is processed and how the decision is made based on the processed arc signal. Two major concerns for the detector are the way to condition the arc signal and the execution of detection algorithm. The decision of utilizing digital signal processor is made since complexity, cost, and hardware debugging effort could be extensive if using analog circuit for such complicated task. Considering the long period of customizing an arc detector and the possible failure because of the design flaw, it's desired to purchase a commercial programmable detector to ease the algorithm development.

Several requirements exist when making the selection. First, there should be appropriately designed peripheral circuit to level and shift the arc signals. Further while digitizing the analog arc signal, the sampling rate and resolution should be high enough in order to preserve arc characteristic. What's more, the embedded processor should have enough computational and storage capability for the realization of arc detection algorithm. Based on the above criterions, Texas Instrument RD-195 is selected as a possible solution.

Texas Instrument RD-195 is an FFT based UL certified arc fault detector capable of recognizing both series and parallel arc [63]. This device is connected in series with the cable of PV systems. Figure 22 shows the picture of RD-195.

Figure 22 Picture of RD-195

On the board a transformer with turns ratio of 1:100 first level up the arc voltage and level down the current and the primary side is serially connected to the PV systems. A voltage signal proportional to the current signal is used in the following processing. On the board a 6-order analog pre-filtering circuitry with 40kHz-100kHz passband which is the preferable region [64] is designed to both filter the inverter noise and amplify the arc signal. At the A/D conversion stage, SM73201 is the ADC chip on the board. It has 16-bit data resolution and max 250 kS/s sampling rate and it's selected based on their assumption that the determinant characteristic for the detection of arc signal falls within 40kHz-100kHz frequency range. TMS320F28033 [65] is the embedded processor and its signal processing ability need to be further explored.

The signal flow diagram of the product is given in Figure 23. The arc signal is conditioned by the impedance match and clamping, and the analog pre-filter circuit. In the

microprocessor, FFT based algorithm is executed to the conditioned and digitized arc signal and the detection decision is made. In its original detection algorithm, the overall detection duration for one cycle lasts 16.82 ms, and during this time 7.25 ms is spent on the data acquisition. Sampling for the arc signal is paused during the rest 9.57 ms, and the possibility of missing an arc signal exists. Therefore the original FFT based detection algorithm of RD-195 doesn't have good real-time characteristic.

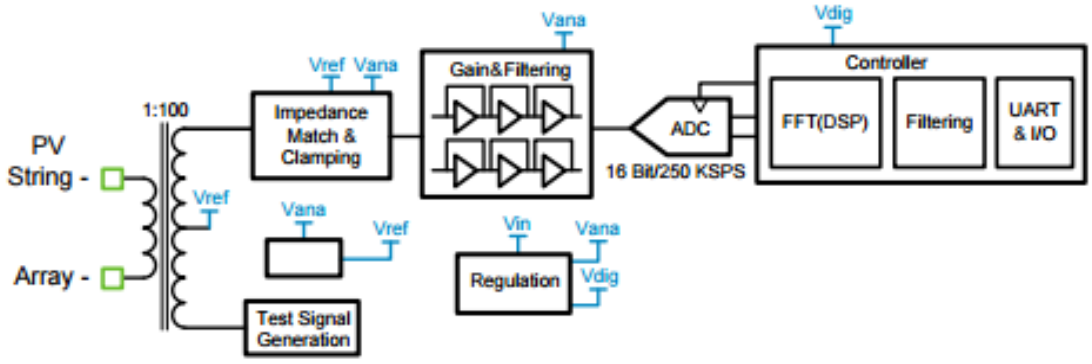

Figure 23 Signal flow of RD-195

As a programmable arc detector, RD-195 eliminates our hardware design challenge and it's expected to transplant the WT algorithm directly on the processor of RD-195. The challenge of pursuing better real-time processing capability is to execute wavelet decomposition algorithm once for every sampling period. Because of the frequency content being focused on is 40 kHz – 100 kHz [66], the least requirement for the sampling rate is 200 kHz in order to preserve enough frequency feature. As a consequence, the allowable time for the algorithm execution is very limited. For the 28033

processor, this requirement corresponds to 10ns or 300 clock cycles for the entire algorithm execution.

4.2 Algorithm development

The limited allowable clock cycles urges us to optimize the detection algorithm code and fully utilize the computational capability. To concur such difficulty, different programming techniques are explored.

First, code generation through MATLAB Simulink embedded target block is used. The compilation of graphical code is accomplished through MATLAB, and an executable file is generated. This method is easiest but wasteful in both program space and CPU resources as the code is compiled inefficiently. Therefore this method is discarded. The expression of how the filter bank is implemented is shown below:

$$Output = Coeff[N] \times Input[1] + Coeff[N-1] \times Input[2] + \cdots + Coeff[1] \times Input[N];$$

$$Input[N] = Input[N-1];$$

$$Input[1] = Input[newest];$$

It's shown in the equation that every data in the input array is moved forward by one when a new input comes in which is unnecessary, therefore the efficiency is reduced by a great extent. With implementation of wavelet filter bank through MATLAB, the max sampling rate can reach up to only 30 kHz with 30% memory used.

Secondly the filter bank is realized through C programming. This method only updates the most recent input and keeps all other data in the same memory location. The difference is the array is indexed using a circular buffer method. The expression of this filter implementation can be expressed as:

$$Output = \sum_i \sum_j Coeff[N - j] \times Input[(i + j)\%N]$$

In the expression, *i* is a counter to index the input array and *j* is a counter to index the coefficient array. By avoiding the data shifting and complicated expression of filter implementation, the time needed for execution and program space are both saved. The filter is implemented in a simple line of code resulting in the minimal memory usage of only 11.5%, however from the test the max sampling rate is only 83.5 kHz which is still far from our 200 kHz expectation. After diving deeper into the ASM code after compilation referring to the CPU instruction set [67], it's found the code looks precise in C but not for the assembly code. "%" which stands for the modular operation in the index computation takes too much computational effort in practice.

As a solution, the filter is implemented through manually controlled indexing. In this method, the filter implementation is described in cases and the amount of cases equals the coefficient length. And in every case, index of the input and coefficient array is given by an integer number. It can be expressed as below:

Case 1: $Output = Coeff[N] \times Input[1] + Coeff[N-1] \times Input[2] + \cdots + Coeff[1] \times Input[N];$

Case 2: $Output = Coeff[N] \times Input[2] + Coeff[N-1] \times Input[3] + \cdots + Coeff[1] \times Input[1];$

$\vdots$

Case N:

$Output = Coeff[N] \times Input[N] + Coeff[N-1] \times Input[1] + \cdots + Coeff[1] \times Input[N-1];$

By making the modification, the program space needed increases to 36% whereas the sampling rate can reach 200 kHz. The reason for the acceleration comes from the

elimination of unnecessary jump and branch instruction. An obvious drawback from this method is the inefficiency and inconvenience of the coding method. However an important introspection from the development process is advanced coding technique may not be optimal for embedded hardware programming and it's the specific application which decides the optimal solution.

In such speed sensitive application, the location of the program affect the execution rate as well. Random Access Memory (RAM) has the fastest read/write access enabling quicker execution but smaller usable memory space; FLASH memory is slower in read/write access by about 25% but contains larger usable storage space. Table 2 listed the time measured for conducting wavelet decomposition of different coefficients and the comparison between the two memory spaces.

Table 2 Comparison between FLASH and RAM execution duration on 28033

Time available(to do two levels decomposition): 2.33 μs			
Coefficients	Num of levels	FLASH	RAM
db3	one	2.80 μs	2.00 μs
	two	3.92 μs	3.68 μs
db4	one	3.08 μs	2.48 μs
	two	4.40 μs	4.24 μs
db5	one	3.24 μs	N/A
	two	5.04 μs	N/A
db6	one	3.52 μs	N/A
	two	5.60 μs	N/A
db7	one	3.86 μs	N/A
	two	6.00 μs	N/A
db8	one	4.06 μs	N/A
	two	6.60 μs	N/A
db9	one	4.72 μs	N/A
	two	7.16 μs	N/A
*N/A suggest information not applicable because of the limitation of program space.			

Excluding the time for data transmission, time available for conducting the wavelet decomposition is 2.33μs in order to realize 200 kHz sampling rate. From table. 2, program space wise, RAM is not capable of handling 2-levels decomposition from db5 coefficient while it's up to 2-levels db9 for FLASH indicating the influence from the available memory space. In terms of executional speed, even with the fastest read/write access, only db3 can be realized with 200 kHz sampling rate. Therefore higher computational capability is needed.

4.3 Hardware upgrade

An idea to solve the problem is to increase the CPU's clock rate. As the CPU is embedded at an integrated board with connection to all kinds of analog data acquisition circuitry, designing a customized board should be the best solution except the extensive effort required. The system schematic of RD-195 revels an important feature of this board: the CPU receives data from the external ADC chip, and all data transmitted from out of the ADC to the CPU is digital data through the serial peripheral interface (SPI) module. Data is sent from the ADC and received at the SPI bit by bit following with the enable and clock signal, and every 16-bits represents a complete data. Therefore alternatively we introduced three necessary digital signal: enable, clock, and data out of the board using wires to an external CPU like the picture shown in Figure 24. In the figure, the upgraded processor is TMS320F28335 [68], and the improvement compared to the 28033 is listed in table 3. After the upgrade, the clock rate is increased by 2.5 times, RAM and FLASH space are increased by 3 times and 8 times correspondingly.

Table 3 Comparison between 28033 and 28335 processor

CPU	Clock Rate	RAM Space (16-bit)	FLASH Space (16-bit)
28033	60M	10K	32K
28335	150M	34K	256K

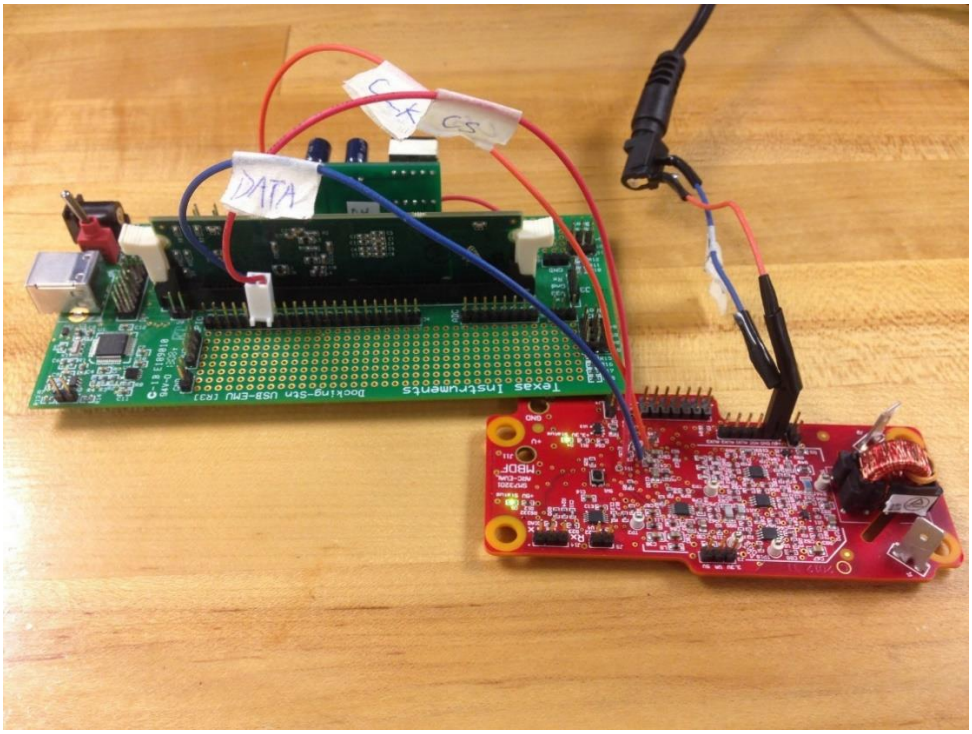

Figure 24 RD-195 with upgraded processor

It still remains to be a problem, however, whether the arc signal is still accurate on the upgraded system. To calibrate the upgraded detector, the digitized arc signal is compared against the analog signal. Figure 25 shows the result before modification to the hardware as a reference and Figure 26 shows the real calibration result. Signal in color blue is the digitized arc signal received on the upgraded processor; in yellow is the analog arc signal before A/D conversion; in purple is the chip selection signal starting the

conversion at the falling edge and the terminating the conversion at rising edge; in green is the clock signal determining the conversion rate of each bit. It's found that through external wiring the signal noise is enlarged but that does not affect with the discrimination of logic high and logic low, and the digitized arc data the processor receives is remained accurate.

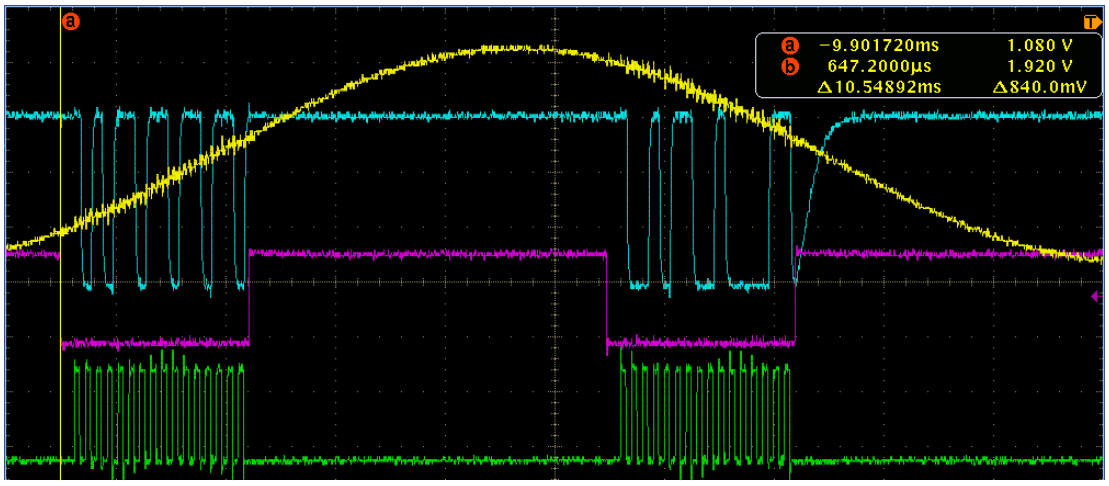

Figure 25 Analog and digitized arc signal on original RD-195

With the improvement of hardware performance, a re-evaluation of wavelet processing ability is needed. Similar to the steps measuring the execution time for 28033, a statistic table is made listing the execution time and frequency bandwidth resulted. Table 4 shows the measurement result for 1-level decomposition and table 5 shows the measurement result for 2-levels decomposition respectively. From the table, the bandwidth that the upgraded processor can handle is increased by about 16 kHz for 1-level

decomposition. Not only 1-level decomposition performance improved, 2-level decomposition can be realized with up do db4 coefficient.

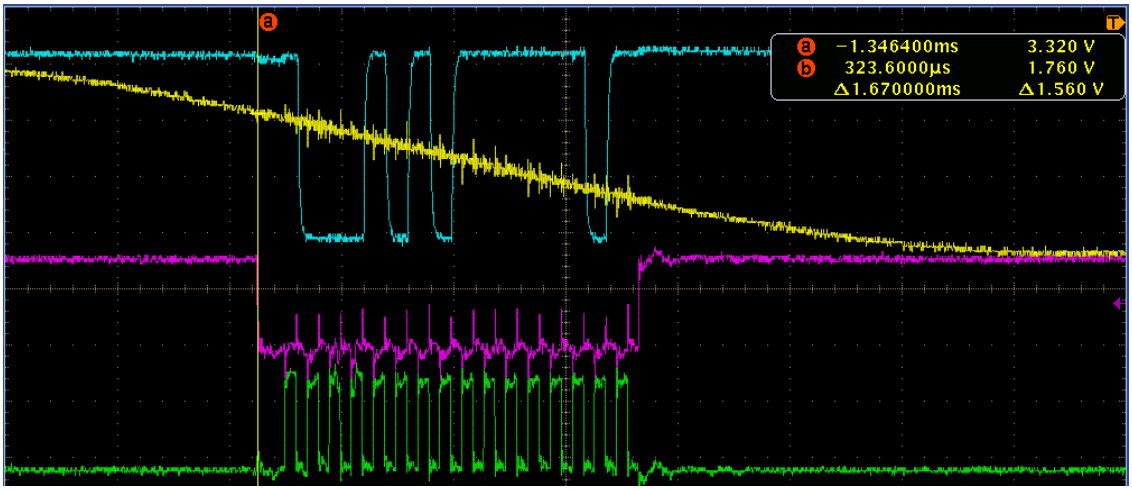

Figure 26 Analog and digitized arc signal on upgraded RD-195

Table 4 Difference of decomposition capability between 28033 and 28335 processor (1-level)

1-Level Wavelet Decomposition				
Coefficients	Processing Time		Resulting Frequency Bandwidth	
	28335	28033	28335	28033
db3	0.99µs	2.8µs	50.6kHz-101.2kHz	33.6kHz-67.2kHz
db4	1.22µs	3.08µs	48.4kHz-96.8kHz	32.1kHz-64.1kHz
db5	1.96µs	3.24µs	44.6kHz-89.2kHz	35.6kHz-61.2kHz
db6	2.72µs	3.52µs	39.4kHz-78.2kHz	29.2kHz-58.4kHz
db7	3.16µs	3.86µs	36.0kHz-72.0kHz	22.9kHz-55.8kHz
db8	3.5µs	4.06µs	33.4kHz-66.8kHz	27.2kHz-54.5kHz

Table 5 Difference of decomposition capability between 28033 and 28335 processor (2-levels)

2-Levels Wavelet Decomposition				
Coefficients	Processing Time		Resulting Frequency Bandwidth	
	28335	28033	28335	28033
db3	1.6μs	3.92μs	23.2kHz-46.3kHz, 46.3kHz-92.6kHz	N/A
db4	2.36μs	4.40μs	19.7kHz-39.4kHz, 39.4kHz-78.8kHz	N/A
db5	4.06μs	5.04μs	N/A	N/A
db6	4.16μs	5.60μs	N/A	N/A
db7	4.24μs	6.00μs	N/A	N/A
db8	4.68μs	6.60μs	N/A	N/A
*N/A suggests frequency range of the 2nd level decomposition falls within the stopband of prefiltering circuit, so this data is not applicable.				

5. REAL-TIME ARC DETECTION

5.1 Threshold setting

A crucial task in the arc detection is the threshold setting for the determination of arcing events. A difficulty from real-time processing is that the internal variable during wavelet decomposition is invisible because RD-195 design is not equipped with a digital-analog-converter (DAC) to help with the visualization of decomposition result.

As a solution, the conditioned arc signal after pre-filtering circuitry can be recorded and utilized in the analysis. In MATLAB, the decomposition process is simulated using the recorded signal which is sampled at 1MHz rate and downsampled by 5 to achieve 200kHz data rate. The arc signal is decomposed using the dyadic tree filterbank in MATLAB and it's expected to find some parameter which can differentiate arcing from a frame of noisy wave including inverter noise.

In the experiment, arc current for the threshold setting doesn't work. By contrast, it's found the power of the arc current signal has a significant increment only from 1st-level decomposition highpass filter covering 50kHz - 100kHz frequency band. Figure 27-29 shows the original waveform and the signal power of 1st-level decomposition highpass filter result. From the figure, the increment appears at somewhere near the start where a sharp current drop is present, and at the end where the arc extinguishes and current immediately raises back to normal. This result meets our expectation as with the existence of the 40kHz - 100kHz bandpass filter, any useful feature at frequency band lower than 40kHz has been greatly attenuated. It's worthwhile to consider setting the detection threshold based on the power increment.

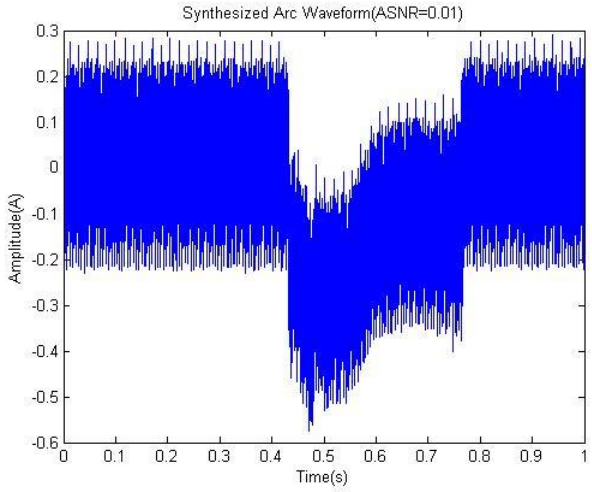

(a) Synthesized arc waveform

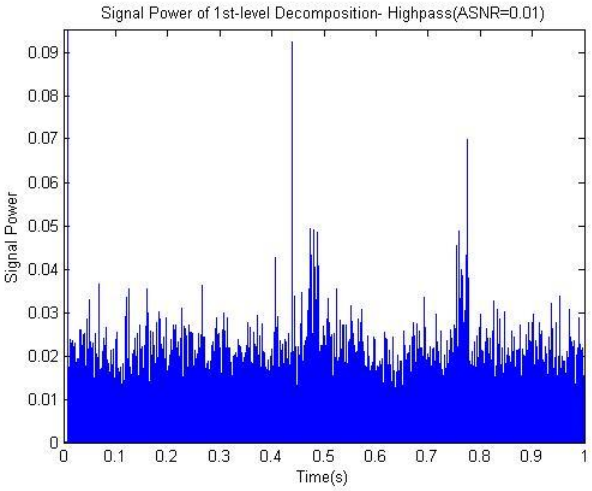

(b) Signal power of 1st-level decomposition highpass result

Figure 27 Arc signal and signal power from 1st-level decomposition (50 kHz – 100 kHz) for ASNR=0.01

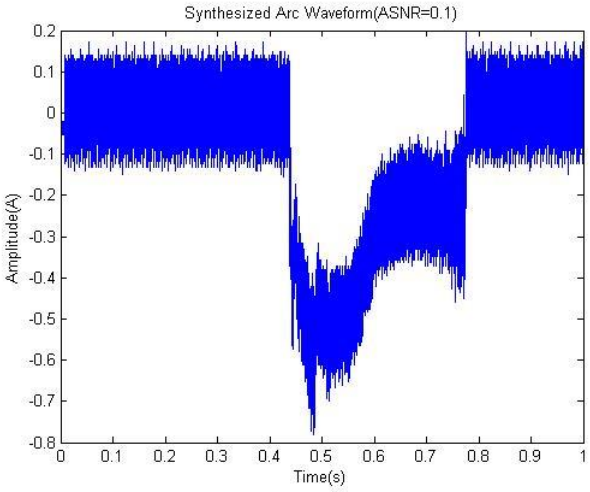

(a) Synthesized arc waveform

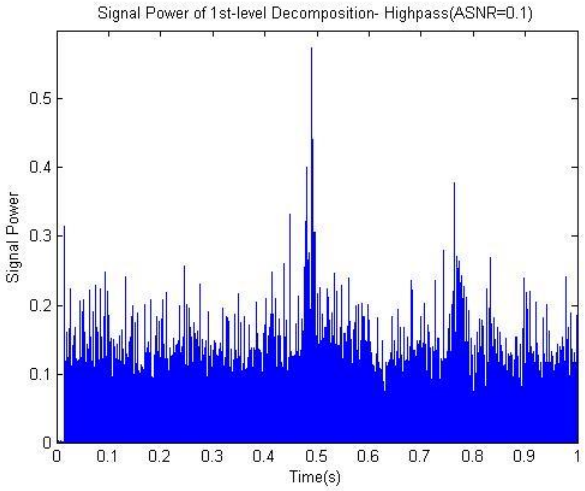

(b) Signal power of 1st-level decomposition highpass result

Figure 28 Arc signal and signal power from 1st-level decomposition (50 kHz – 100 kHz) for ASNR=0.1

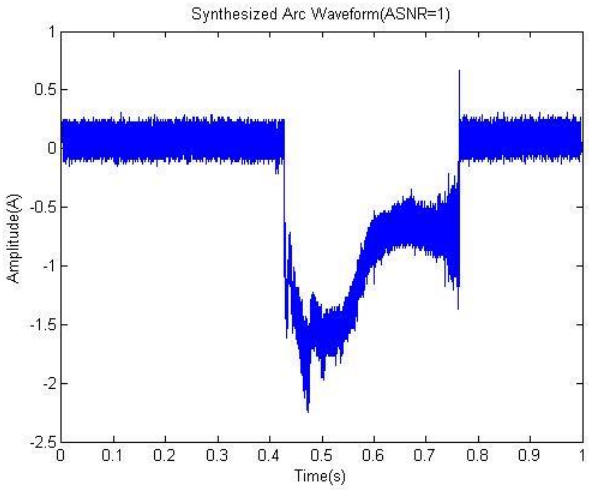

(a) Synthesized arc waveform

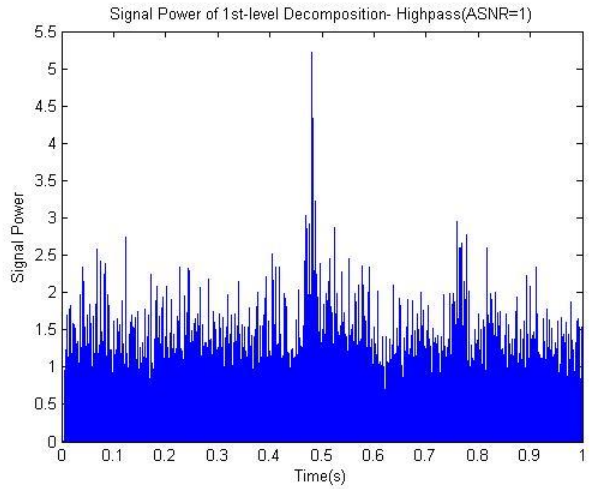

(b) Signal power of 1st-level decomposition highpass result

Figure 29 Arc signal and signal power from 1st-level decomposition (50 kHz – 100 kHz) for ASNR=1

Another observation from the simulated result, is the absolute value of the decomposed signal power is varying proportionally with the ASNR value and hence

threshold setting relying on the absolute value is not appropriate. However from the result the duration and ratio of power increment compared to normal inverter noise looks similar for all three tested ASNR, so the relative increment could be considered as the threshold setting parameter.

Another simulation is conducted to see the detection result with the power ratio threshold setting. To avoid the nuisance tripping due to the spikes, instead of single points the decision is made using the average power of a detection frame. Each detection frame contains 128 points, and arc is determined if the average power of detection frame exceeds the threshold consecutively 2 times. Threshold is set to be 1.4 based on the system power reference. This value is set with the expectation that arcs are detected as possible with no nuisance tripping. Arc signals could be missed if the threshold is set to be too high and normal inverter noise might be regarded as arc signal if it is too low. The average of first 32 frames of data when no arc happens is used as reference of the system. The reason to compute 128 points for each detection frame and 32 frames is to reduce the calculation requirement for processor. In this situation, the average value can be derived through binary left shift instead of doing division operation which consumes a lot CPU resource for fixed point processor. In the simulation, coefficient from db3 to db9 are all tested, and it's found the db3 is enough for the detection while db9 doesn't provide much improvement.

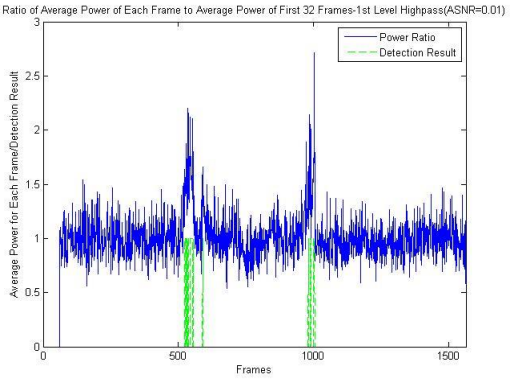

(a) Simulated detection result for ASNR=0.01

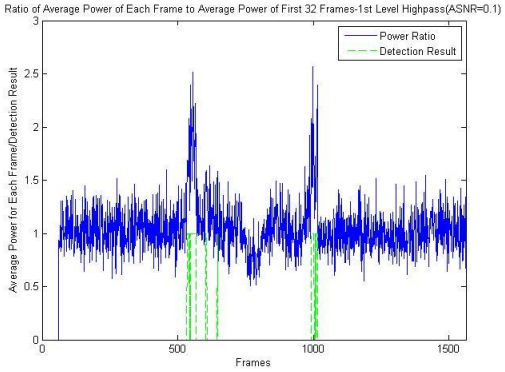

(b) Simulated detection result for ASNR=0.1

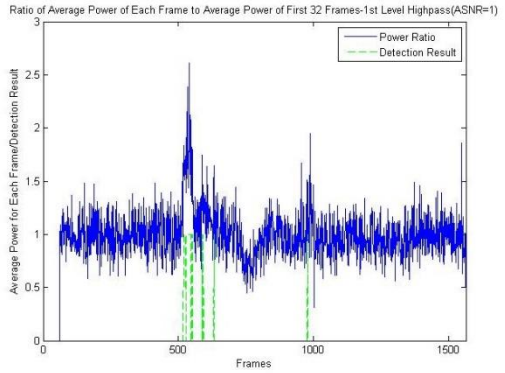

(c) Simulated detection result for ASNR=1

Figure 30 Simulative detection result using 1.4 times threshold for ASNR=0.01, 0.1, and 1

The detection process is simulated in MATLAB and the result is shown in Fig 30. In the result, the cluster of logic high shown in green color indicate the moment when arc is determined. Just as expected, by setting the 1.4 threshold almost the overall duration where the average signal power has obvious relative increment is covered. Some points in between where the arc is sustained while the power doesn't exhibit noticeable increment can be detected as well. For the synthesized signal used in the study, even the sustained arc can't be completely determined the two continuous cluster of logic high displays enough feature for the arc detection.

5.2 Real-time arc detection using synthesized arc signal

With the reference of a successful detection in MATLAB simulation, the real time detection is programmed on hardware. The hardware detection has three steps: initialization of the detection to obtain the average signal power for the system, calculating the power of each detection frame, and presenting the detection result through the LED indicator. If an arc is detected the LED will light up and vice versa.

In the program, the data acquisition is triggered by CPU timer interrupt once every 750 clock cycles which means 200 kHz sampling rate corresponding to the upgraded 28335 processor. In the CPU interrupt routine, SPI module works under master input slave output (MISO) mode and two general purpose input/output (GPIO) pin are configured to send out chip selection and clock signal. Another GPIO pin receives digitized arc signal bit by bit. The SPI interrupt routine will be triggered once the 16-bit digital data transmission is complete which indicates the accomplishment of one sampling period. Inside the SPI interrupt routine is the wavelet decomposition and the decision making

algorithm and the next data sampling happens when the CPU timer counter reaches 750. This detection technique runs in a forever going ‘for’ loop and continues monitoring the arcing status of the PV systems.

The real-time arc detection is conducted for synthesized arc signal with ASNR=0.01, 0.1, and 1. Figure 31 shows the result with yellow signal being input waveform and blue signal being the detection output. This result of real-time experiment meets our expectation from the MATLAB simulation that two clusters of logic high can be observed suggesting the successful detection of the arc signal. It further justifies the method of visualization through MATLAB simulation when not enough hardware resources are provided.

The FFT based detection algorithm that come along with original RD-195 is compared against the wavelet detection technique. In the experiment, the LED indicator on the RD-195 lights up for all three tested ASNR indicating the good detection performance. However if observing the moment when the detection result is given, it’s found that arc is detected before happening. As a comparison, inverter noise is sent for detection and same result is obtained. From the detection result, the good detection performance can be explained as nuisance tripping. The result is shown in Figure 32 and in the figure result of ASNR=0.01 is given as an example.

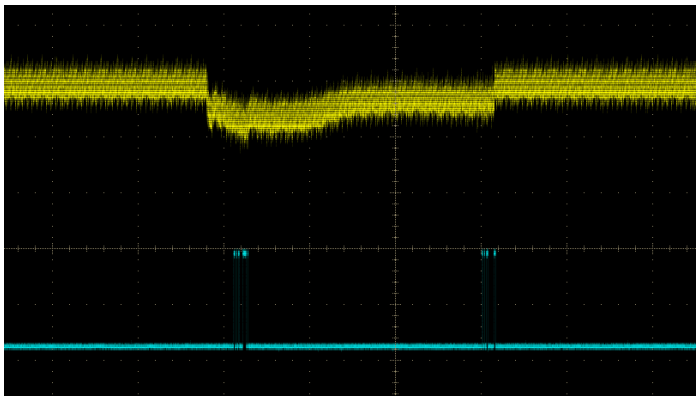

(a) Real-time detection with synthesized arc for ASNR=0.01

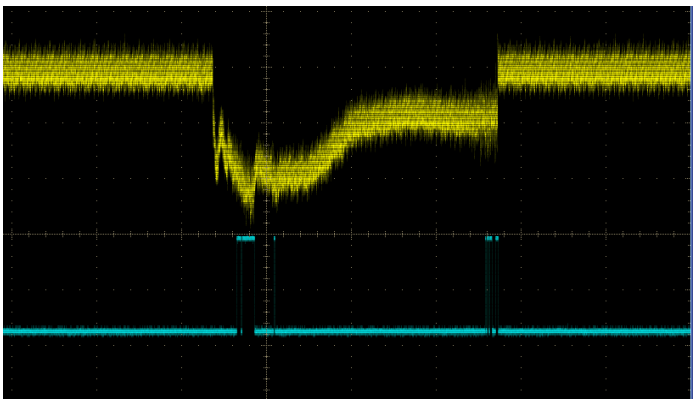

(b) Real-time detection with synthesized arc for ASNR=0.1

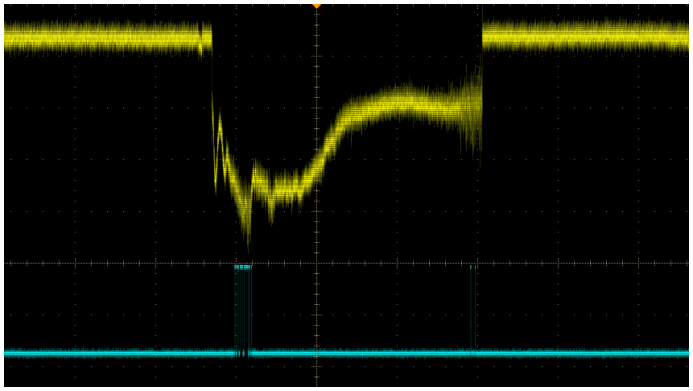

(c) Real-time detection with synthesized arc for ASNR=1

Figure 31 Real-time detection with synthesized arc for ASNR=0.01, 0.1, and 1

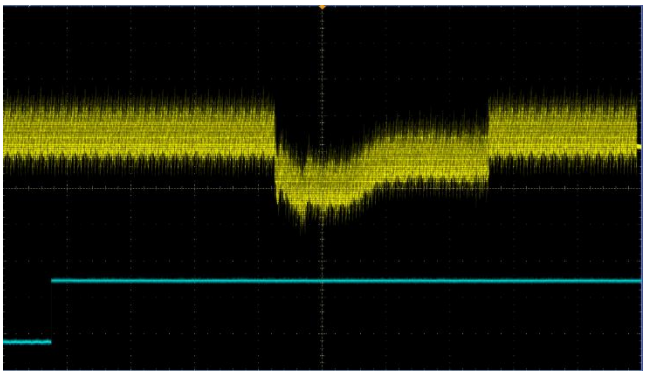

(a) Real-time detection result of ASNR=0.01 for FFT based algorithm

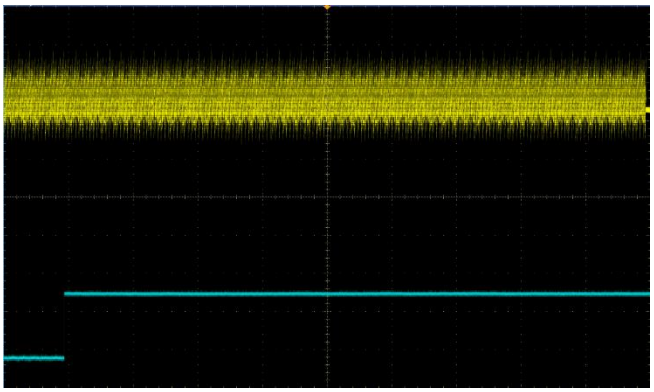

(b) Real-time detection result of inverter noise for FFT based algorithm

Figure 32 Real-time detection result for FFT based algorithm

5.3 Real-time arc detection using real PV arc signal

Efficacy of the wavelet based arc fault detection technique is verified using synthesized arc signal through real-time experiment, however it's still doubtful whether the detection technique applies to the real arc happened on the operating PV systems. For further verification, tests are done to four sets of real PV arc signal and inverter noise acquired from Sandia National Laboratory. Data 1-3 are obtained from PV system equipped with different inverters and Data 3-4 are acquired from the same system but in different time.

Figure 33 shows the source data plotted in MATLAB with blue line being the inverter noise and red line being the arc signal. The arc happens when the abrupt current drop starts.

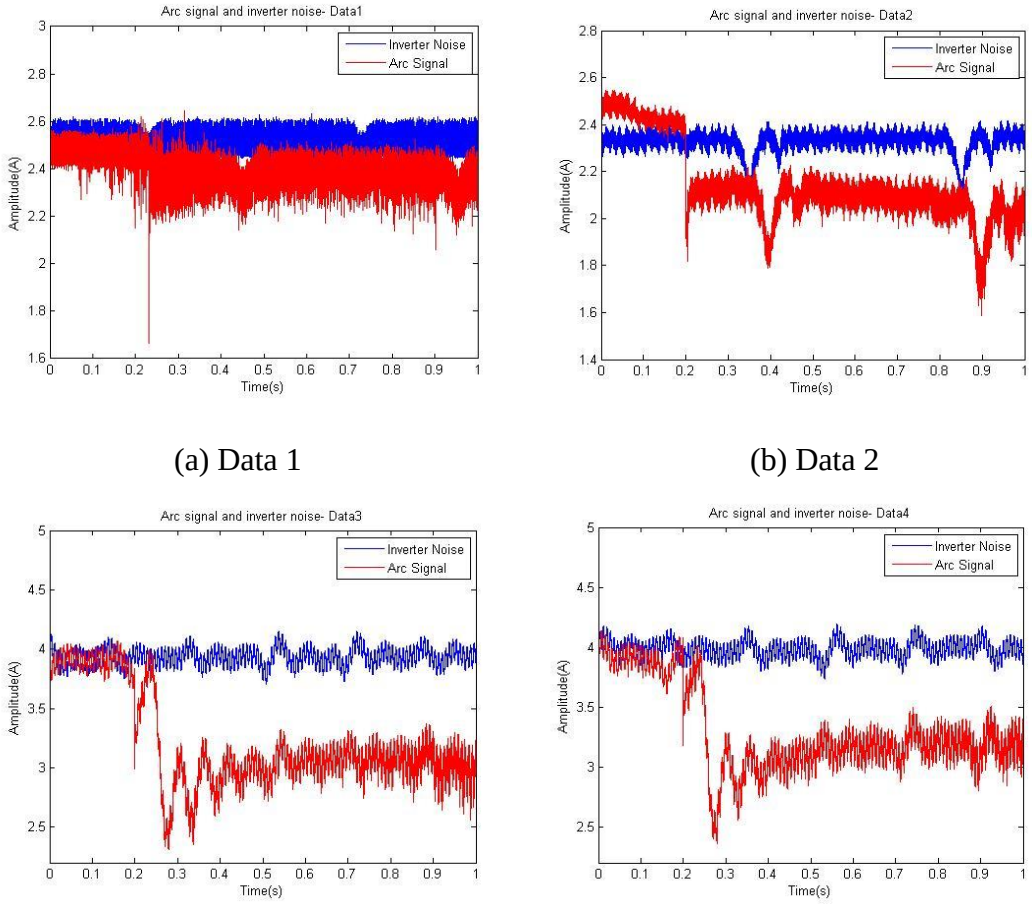

(a) Data 1 (b) Data 2

(c) Data 3 (d) Data 4

Figure 33 Real PV arc data (inverter noise included) and inverter noise

The detection result using wavelet algorithm is shown in Figure 34. Signal in yellow color represents arc signal and signal in blue is detection result, inverter noise is

not shown. The arc is detected from the moment where it begins, at the same time no nuisance tripping is caused due to the inverter noise.

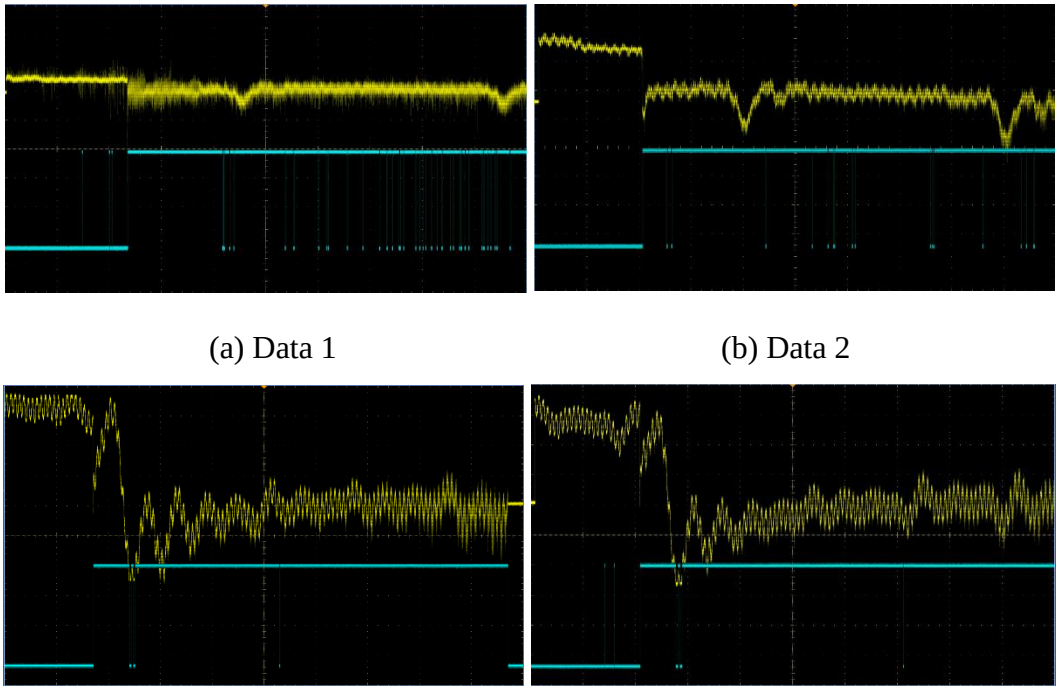

(a) Data 1 (b) Data 2

(c) Data 3 (d) Data 4

Figure 34 Wavelet algorithm detection result for real PV arc signal

There might be some irregularities that several moments when only inverter noise exists are determined as arcing event but it's unavoidable as the possibility of other unknown noise still exists. In the sustained arcing duration, arc is detected continuously. Still, there're some abnormal points where arc are not detected. Part of the reason could be the arc's naturally unstable characteristic that the determination criterion isn't always

met, but it's also possible that the detection technique is not developed perfectly and there's still room for further improvement.

FFT based algorithm is tested for the four sets of arc data as comparison. The detection result is shown in Figure 35, arc is detected for all data sets seemingly suggesting the effectiveness of their detection technique, however it seems still the determination starts earlier than the occurrence of actual arcing event.

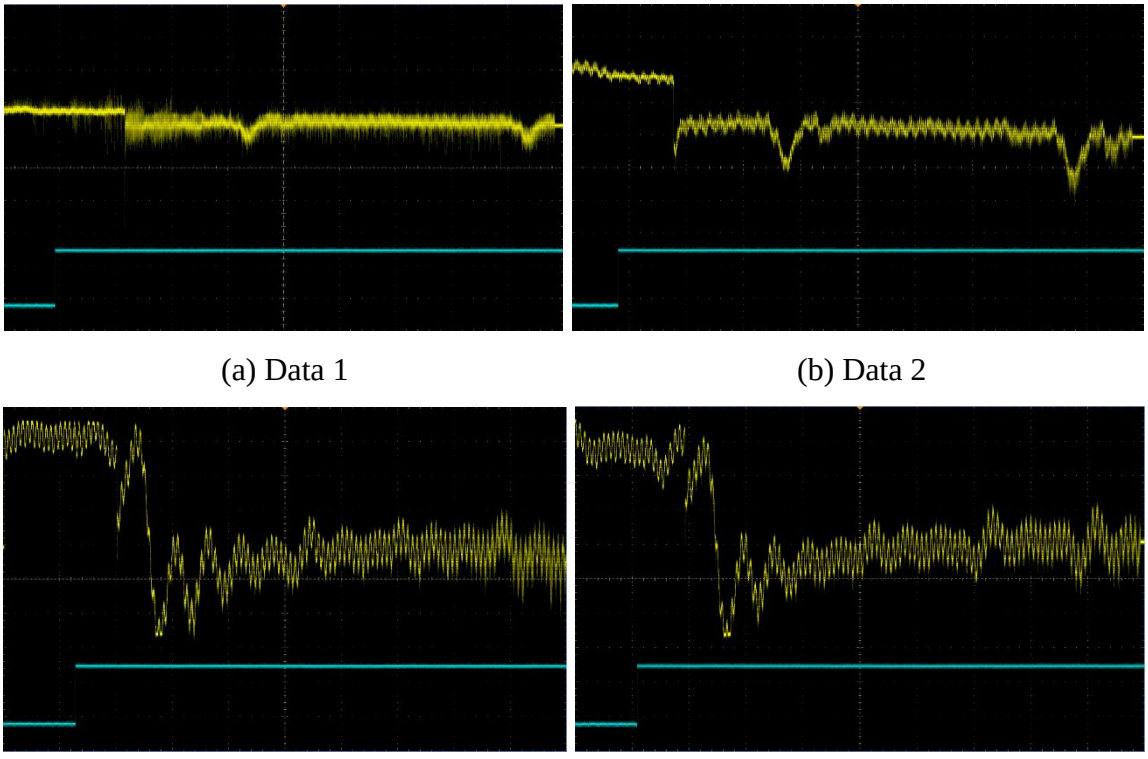

(a) Data 1 (b) Data 2

(c) Data 3 (d) Data 4

Figure 35 FFT algorithm detection result for real PV arc signal

To check if it represents the correct detection result, four corresponding inverter noise are tested. Figure 36 shows the detection result, just as expected the good detection performance is essentially nuisance tripping.

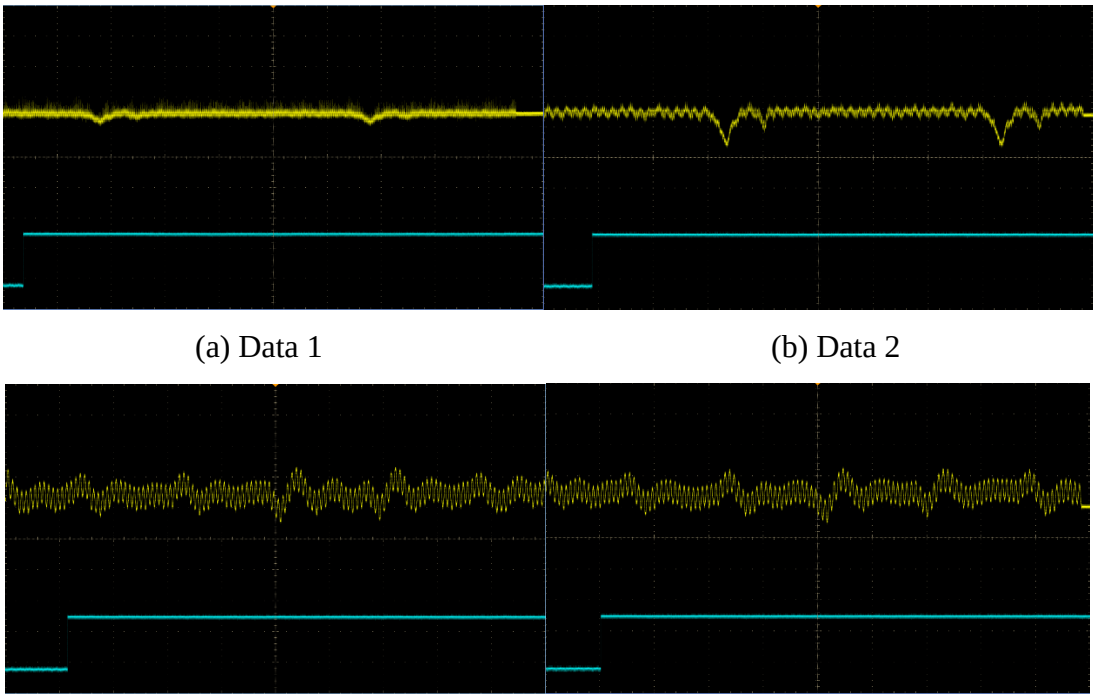

(a) Data 1 (b) Data 2

(c) Data 3 (d) Data 4

Figure 36 FFT algorithm detection result for inverter noise

To find out the reason, the FFT algorithm on RD-195 is further explored. In the algorithm, the sampling frame contains 1024 points sampled at 238kHz rate and the algorithm conduct 1024 points FFT after applying the Hanning Window to the time domain sample. In the frequency domain, 45kHz - 75kHz frequency band of interests is divided into lower half and higher half evenly, and the unwanted frequency bin magnitude

value is excluded by discarding several largest and smallest value. A parameter band summation is derived by adding the weighted lower and higher magnitude. Finally the arc is determined if the logarithm of the properly scaled band summation exceeds the threshold.

This detection technique is developed by Texas Instruments and the technique of frequency information processing after FFT as well as the weighting or scaling factor utilized in the algorithm could be derived based on their arc data statistic and analysis. The algorithm is simply denied by the nuisance tripping of PV inverter data given from Sandia National Lab and there could be some flaws in its FFT detection algorithm so that it's not universally applicable. However without large amount of arc data, it's not legitimate to criticize or judge the effectiveness of this algorithm.

Another difference worth mentioning between Texas Instrument's FFT algorithm and wavelet decomposition method developed by us, is their lacking of self-adjustability. Even though the detection criterion is programmable before operating on PV system, it's invariable once executing. It's possible that the environmental influence or adjustment on the load side changes the frequency feature of the PV current and induces the detection failure. For the wavelet based detection decision is made based on the relative increment to the referential system power, and in the future the program can be reset once a while to keep up with the operating status change. In this way, for wavelet detection algorithm the threshold can be updated with the variation of operating condition while it's impossible for FFT based algorithm to form a new detection criterion without being disconnected from the system.

6. CONCLUSION AND FUTURE WORK

Arc fault is one of the major safety concerns for the reliable operation of DC PV system induced by loose conduction and insulation deterioration, etc. It can occur anywhere in the system and failure of arc detection may cause system instability, property loss, or even human injury. In time domain, the amplitude of arc current may not be able to trigger the protection device and it doesn't exhibit zero current crossing property like AC systems. In the frequency domain, a complication for the arc detection is the PV arc can be easily disguised by the existence of the inverter noise. Further for the frequency analysis method, Fourier based techniques has the trade-offs between frequency resolution and temporal localization and is not suitable for non-stationary and non-periodic arc signals.

Wavelet transform in comparison, is more appropriate for its adjustable analysis window size. It approximates a signal using finite energy short duration wavelets derived from a base wavelet after different dilation and translation. Daubechies coefficient is used in the study and discrete wavelet transform is implemented through a quadrature mirror filter. The filter coefficient is proportional to the wavelet analysis performance, more complex wavelets have better capability characterizing a signal whereas more computational effort on hardware is expected.

In order to represent the arc signal of different power levels on the PV systems, the concept of Arc-Signal-Noise-Ratio is introduced. It describes an arc signal by the power ratio against the inverter noise of the PV systems. Composite arc signal with

ASNR=0.01, 0.1, and 1 are synthesized using lab generated arc and recorded PV inverter noise.

The theoretic arc study using synthesized arc signal for FFT and WT are compared. FFT algorithm can't distinguish arcing from non-arcing based on the frequency characteristic, nor to say the temporal localization. WT by contrast shows the increment of current magnitude at the highpass filter result of 7^{th}-level decomposition.

A high fidelity arc study testbed is constructed for the reproduction of the arc signal. The arc current is reproduced through the digital to analog conversion following by the power amplification. Frequency sweep covering 10kHz – 160kHz is conducted by an automation program to ensure no distortion during the reproduction. The unity gain system is built upon the testbed so that the reproduced arc has same power as the originally recorded arc. Development of the GUI improves the efficiency of the arc study.

RD-195 is chosen as the detection hardware and different programming techniques are tested in the realization of wavelet decomposition algorithm. After the upgrade of processor, 2-levels decomposition can be realized with 200kHz sampling rate which satisfies our requirement to execute detection algorithm for every sampling duration.

Due to the hardware limitation, threshold setting is done by the assistance of MATLAB simulation. Instead of the current amplitude, ratio of the current signal power compared to system referential power at 1.4 is found to be an appropriate threshold setting.

The real-time detection comparison of FFT against WT is conducted using both synthesized arc signal and real PV arc signal. WT based detection algorithm is able to successfully detect synthesized arc signal as expected, and it's further validated through

the good detection performance when applying real PV arc signal. In comparison, the fact that the positive detection result of FFT detection technique is essentially nuisance tripping indicates the possible flaws in the algorithm. In the study, WT based algorithm can be successfully realized on a commercially available detection hardware and it displays better detection performance. As a conclusion WT is more suitable than FFT in the DC arc fault detection.

This project can be further extended in several aspects. First, a DC arc library can be established including large quantities of arcing event and inverter noise signal so researchers can apply the ASNR concept and improve the threshold setting technique based on a high volume statistics. Moreover, an arc study platform with higher hardware capability can be constructed that in the detection technique development stage researchers won't be constrained by practical hardware limitation. Last but not least, the commercialization of wavelet based detection technique with its customized hardware design.

REFERENCES

[1] M. Wendl, M. Weiss, and F. Berger, "HF Characterization of Low Current DC Arcs at Alterable Conditions," in *Proceedings of the 27th International Conference on Electrical Contacts (ICEC)*, 2014, pp. 1-6.

[2] C. Strobl and P. Meckler, "Arc Faults in Photovoltaic Systems," in *Proceedings of the 56th IEEE Holm Conference on Electrical Contacts (HOLM)*, 2010, pp. 1-7.

[3] R. H. Lee, "The Other Electrical Hazard: Electric Arc Blast Burns," *IEEE Trans on Industry Applications*, vol. IA-18, pp. 246-251, 1982.

[4] A. Braverman. (2006). *The Truth About Arc Detection*. Available: http://www.evaluationengineering.com/articles/200603/the-truth-about-arc-detection.php

[5] J. Yuventi, "DC Electric Arc-Flash Hazard-Risk Evaluations for Photovoltaic Systems," *IEEE Trans on Power Delivery*, vol. 29, pp. 161-167, 2014.

[6] J. Johnson, "Overview of Arc-Faults and Detection Challenges," Sandia National Laboratories, 2011.

[7] T. Zgonena, L. Ji, and D. Dini, "Photovoltaic DC Arc-Fault Circuit Protection and UL Subject 1699B," Underwriters Laboratories Inc (UL), 2011.

[8] Z. Meng, L. Wang, and Q. Sun, "The characteristics of DC arc faults current," in *15th European Conference on Power Electronics and Applications (EPE)*, 2013, pp. 1-9.

[9] M. Davarifar, A. Rabhi, and A. E. Hajjaji, "Comprehensive Modulation and Classification of Faults and Analysis Their Effect in DC Side of Photovoltaic System," *Energy and Power Engineering*, vol. 5, 2013.

[10] H. Trabish. (2013). *Putting Out the Solar-Panel Fire Threat*. Available: http://www.greentechmedia.com/articles/read/Putting-Out-The-Solar-Panel-Fire-Threat

[11] M. K. Alam, F. Khan, J. Johnson, and J. Flicker, "A Comprehensive Review of Catastrophic Faults in PV Arrays: Types, Detection, and Mitigation Techniques," *IEEE Journal of Photovoltaics*, vol. 5, pp. 982-997, 2015.

[12] F. Erhard and F. Berger, "Measurements of DC arc faults in real photovoltaic systems," in *48th International Universities Power Engineering Conference (UPEC)* 2013, pp. 1-6.

[13] J. Flicker and J. Johnson, "Electrical simulations of series and parallel PV arc-faults," in *39th IEEE Photovoltaic Specialists Conference (PVSC)*, 2013, pp. 3165-3172.

[14] J. Johnson, M. Montoya, S. McCalmont, G. Katzir, F. Fuks, J. Earle, *et al.*, "Differentiating series and parallel photovoltaic arc-faults," in *38th IEEE Photovoltaic Specialists Conference (PVSC)*, 2012, pp. 000720-000726.

[15] B. G. Jay Johnson, Andrew Meares, Armando Frequez, "Series and Parallel Arc-Fault Circuit Interrupter Tests," Sandia National Laboratories, 2013.

[16] J. Johnson and K. Armijo, "Parametric study of PV arc-fault generation methods and analysis of conducted DC spectrum," in *40th IEEE Photovoltaic Specialist Conference (PVSC)*, 2014, pp. 3543-3548.

[17] G. Artale, A. Cataliotti, V. Cosentino, and G. Privitera, "Experimental characterization of series arc faults in AC and DC electrical circuits," in *IEEE International Instrumentation and Measurement Technology Conference (I2MTC) Proceedings*, 2014, pp. 1015-1020.

[18] A. Lazkano, J. Ruiz, E. Aramendi, and L. A. Leturiondo, "Evaluation of a new proposal for arcing fault detection method based on wavelet packet analysis," in *Power Engineering Society Summer Meeting*, 2001, pp. 1328-1333.

[19] M. Rabla, E. Tisserand, P. Schweitzer, and J. Lezama, "Arc Fault Analysis and Localisation by Cross-Correlation in 270 V DC," in *59th IEEE Holm Conference on Electrical Contacts*, 2013, pp. 1-6.

[20] B. M. Aucoin and B. D. Russell, "Distribution High Impedance Fault Detection Utilizing High Frequency Current Components," *IEEE Power Eng Review* vol. PER-2, pp. 46-47, 1982.

[21] B. D. Russell, K. Mehta, and R. P. Chinchali, "An arcing fault detection technique using low frequency current components-performance evaluation using recorded field data," *IEEE Trans on Power Delivery*, vol. 3, pp. 1493-1500, 1988.

[22] C. Benner, P. Carswell, and B. Don Russell, "Improved algorithm for detecting arcing faults using random fault behavior," *Electric Power Systems Research*, vol. 17, pp. 49-56, 1989.

[23] NFPA70, "Article 690- Solar Photovoltaic Systems of National Electric Code," 2011.

[24] G. D. Gregory and G. W. Scott, "The arc-fault circuit interrupter, an emerging product," in *IEEE Industrial and Commercial Power Systems Technical Conference*, 1998, pp. 48-55.

[25] D. Lee, A. Trotta, and W. King, Jr., "New Technology for Preventing Residential Electrical Fires: Arc-Fault Circuit Interrupters (AFCIs)," *Fire Technology*, vol. 36, pp. 145-162, 2000.

[26] R. F. Dvorak and K. B. Wong, "Arc Fault Circuit Interrupter System," U.S. Patent 7,253,637 B2, Aug 7, 2007.

[27] X. Zhou, J. J. Shea, J. C. Engel, K. L. Parker, and T. J. Miller, "Arc Fault Circuit Interrupter and Method of Parallel and Series Arc Fault Detection," U.S. Patent 7,558,033 B2, Jul. 7, 2007.

[28] R. T. West, "Photovoltaic Power System with Distributed Photovoltaic String to Polyphase AC Power Converters," U. S. Patent 8,648,498 B1, Feb. 11, 2014.

[29] P. Ward, "Apparatus for Testing an Arc Fault Detector," U. S. Patent 2014/0009163 A1, Jan. 9, 2014.

[30] H. Behrends, M. Kratochvil, M. Hopf, and S. Bieniek, "Method and System for Detecting an Arc Fault in a Power Circuit," U. S. Patent 2014/0062500 A1, Mar. 6, 2014.

[31] C. J. Luebke and B. Pahl, "Method and Apparatus for Enhancing Arc Fault Signal for Detection in Photovoltaic System," U. S. Patent 2014/0055900 A1, Feb. 27, 2014.

[32] Underwriters Laboratories, "UL1699B- Outline of Investigation for Photovoltaic (PV) DC Arc-Fault Circuit Protection", 2013.

[33] A. V. Oppenheim, R. W. Schafer, and J. R. Buck, *Discrete-time signal processing* vol. 2: Prentice hall Englewood Cliffs, NJ, 1989.

[34] J. G. Proakis, "Digital signal processing: principles, algorithms, and application-3/E," 1996.

[35] W. Zhan, S. McConnell, R. S. Balog, and J. Johnson, "Arc fault signal detection - Fourier transformation vs. wavelet decomposition techniques using synthesized data," in *40th IEEE Photovoltaic Specialist Conference (PVSC)*, 2014, pp. 3239-3244.

[36] K. H. Kashyap and U. J. Shenoy, "Classification of Power System Faults Using Wavelet Transforms and Probabilistic Neural Networks," in *International Symposium on Circuits and Systems*, 2003, pp. 423 - 426.

[37] W. Zhan and R. S. Balog, "Arc fault and flash detection in DC photovoltaic arrays using wavelets," in *39th IEEE Photovoltaic Specialists Conference (PVSC)*, 2013, pp. 1619-1624.

[38] S. McConnell, W. Zhan, R. S. Balog, and J. Johnson, "Evaluation method for arc fault detection algorithms," in *40th IEEE Photovoltaic Specialist Conference (PVSC)*, 2014, pp. 3201-3206.

[39] J. Liu and P. Pillay, "An insight into power quality disturbances using wavelet multiresolution analysis," *IEEE Power Engineering Review,* vol. 19, pp. 59-60, 1999.

[40] Y. Weon-Ki and M. J. Devaney, "Power measurement using the wavelet transform," in *Conference Proceedings of IEEE Instrumentation and Measurement Technology Conference, IMTC*, 1998, pp. 801-806 vol.2.

[41] S. Santoso, E. J. Powers, and W. M. Grady, "Power quality disturbance data compression using wavelet transform methods," *IEEE Trans on Power Delivery,* vol. 12, pp. 1250-1257, 1997.

[42] V. L. Pham and K. P. Wong, "Wavelet-transform-based algorithm for harmonic analysis of power system waveforms," *IEEE Proceedings of Generation, Transmission and Distribution,* vol. 146, pp. 249-254, 1999.

[43] L. Eren and M. J. Devaney, "Calculation of power system harmonics via wavelet packet decomposition in real time metering," in *Proceedings of the 19th IEEE Instrumentation and Measurement Technology Conference*, 2002, pp. 1643-1647 vol.2.

[44] H. R. Rosa Fernandez, "An Overview of Wavelet Transforms Application in Power Systems," *14th PSCC,* 2002.

[45] P. K. Ray, S. R. Mohanty, and N. Kishor, "Disturbance detection in grid-connected distributed generation system using wavelet and S-transform," *Electric Power Systems Research,* vol. 81, pp. 805-819, 2011.

[46] G. Wenzhong and N. Jiaxin, "Wavelet-Based Disturbance Analysis for Power System Wide-Area Monitoring," *IEEE Trans on Smart Grid,* vol. 2, pp. 121-130, 2011.

[47] A. Borghetti, S. Corsi, C. A. Nucci, and M. Paolone, "On the Use of Continuous-Wavelet Transform for Fault Location in Distribution Power Systems," *15th Power Systems Computation Conference,* vol. 28 pp. 608-617, 2006.

[48] L. Wen-jun and L. Yuan-chun, "Arc Fault Detection Based on Wavelet Packet," in *4th International Conference on Machine Learning and Cybernetics*, 2005, pp. 1783 - 1788.

[49] H. Zhang, T. Chen, and W. Li, "Arc Fault Signatures Detection on Aircraft Wiring System," in *6th World Congress on Intelligent Control and Automation*, 2006, pp. 5548 - 5552.

[50] Z. Weiyan and W. Weilin, "Detecting low-voltage arc fault based on lifting multiwavelet," in *Asia-Pacific Conference on Computational Intelligence and Industrial Applications,* 2009, pp. 254-257.

[51] M. Misiti, Y. Misiti, G. Oppenheim, and J.-M. Poggi, "Matlab Wavelet Toolbox User's Guide. Version 3," 2004.

[52] A. W. Galli, G. T. Heydt, and P. F. Ribeiro, "Exploring the power of wavelet analysis," *IEEE Computer Applications in Power,* vol. 9, pp. 37-41, 1996.

[53] D. Chanda, N. K. Kishore, and A. K. Sinha, "Application of wavelet multiresolution analysis for classification of faults on transmission lines," in *Conference on Convergent Technologies for the Asia-Pacific Region, TENCON*, 2003, pp. 1464-1469 Vol.4.

[54] S. Narasimhan, N. Basumallick, and S. Veena, *Introduction to wavelet transform: a signal processing approach*: Alpha Science International, Ltd, 2011.

[55] W. David Chan Tat and Y. Xia, "A novel technique for high impedance fault identification," *IEEE Trans on Power Delivery,* vol. 13, pp. 738-744, Jul 1998.

[56] A. N. Akansu and R. A. Haddad, *Multiresolution signal decomposition: transforms, subbands, and wavelets*: Academic Press, 2001.

[57] I. Daubechies, *Ten lectures on wavelets* vol. 61: SIAM, 1992.

[58] C. Luebke, T. Pier, B. Pahl, D. Breig, and J. Zuercher, "Field test results of DC arc fault detection on residential and utility scale PV arrays," in *37th IEEE Photovoltaic Specialists Conference (PVSC)*, 2011, pp. 001832-001836.

[59] Y. Xiu, J. Shengchang, L. Herrera, and W. Jin, "DC Arc Fault: Characteristic Study and Fault Recognition," in *1st International Conference on Electric Power Equipment - Switching Technology (ICEPE-ST)*, 2011, pp. 387-390.

[60] Y. Xiu, L. Herrera, H. Yi, and W. Jin, "The Detection of DC Arc Fault: Experimental Study and Fault Recognition," in *27th Applied Power Electronics Conference and Exposition (APEC)*, 2012, pp. 1720-1727.

[61] Y. Xiu, L. Herrera, J. Shengchang, Z. Ke, and W. Jin, "Characteristic Study and Time-Domain Discrete- Wavelet-Transform Based Hybrid Detection of Series DC Arc Faults," *IEEE Trans on Power Electron*, vol. 29, pp. 3103-3115, 2014.

[62] Y. Liu, S. Ji, J. Wang, X. Yao, and Y. Zhu, "Study on characteristics and detection of DC arc fault in power electronics system," in *International Conference on Condition Monitoring and Diagnosis (CMD)*, 2012, pp. 1043-1046.

[63] C. Oberhauser, F. Boico. (2012). *SM73201 DC Arc Detection Evaluation Board*. Available: http://www.ti.com/lit/ug/snoa564f/snoa564f.pdf

[64] S. Gab-Su, C. Bo-Hyung, and L. Kyu-Chan, "Photovoltaic module-level DC-DC converter with arc fault protection scheme for DC distribution system," in *IEEE ECCE Asia Downunder (ECCE Asia)*, 2013, pp. 917-923.

[65] Texas Instruments. (2013). *Piccolo Microcontrollers*. Available: http://www.ti.com/lit/ug/snoa564f/snoa564f.pdf

[66] B. Novak. (2012). *Implementing Arc Detection in Solar Applications: Achieving Compliance with the new UL 1699B Standard*. Available: http://www.ti.com/lit/ug/snoa564f/snoa564f.pdf

[67] Texas Instruments. (2015). *TMS320C28x CPU and Instruction Set Reference Guide*. Available: http://www.ti.com/lit/ug/snoa564f/snoa564f.pdf

[68] Texas Instruments. (2012). *Digital Signal Controllers (DSCs)*. Available: http://www.ti.com/lit/ug/snoa564f/snoa564f.pdf